Monthly Notices
of the
ROYAL ASTRONOMICAL SOCIETY

Mon. Not. R. Astron. Soc. **416,** 601–617 (2011) doi:10.1111/j.1365-2966.2011.19083.x

Simulations of the formation and evolution of isolated dwarf galaxies – II. Angular momentum as a second parameter

J. Schroyen,★ S. De Rijcke, S. Valcke,★† A. Cloet-Osselaer and H. Dejonghe

Sterrenkundig Observatorium, Ghent University, Krijgslaan 281, S9, 9000 Gent, Belgium

Accepted 2011 May 14. Received 2011 April 13; in original form 2010 December 14

ABSTRACT

We show results based on a large suite of *N*-body/smoothed particle hydrodynamics simulations of isolated, flat dwarf galaxies, both rotating and non-rotating. The main goal is to investigate possible mechanisms to explain the observed dichotomy in radial stellar metallicity profiles of dwarf galaxies: dwarf irregulars (dIrrs) and flat, rotating dwarf ellipticals (dEs) generally possess flat metallicity profiles, while rounder and non-rotating dEs show strong negative metallicity gradients.

These simulations show that flattening by rotation is key to reproducing the observed characteristics of flat dwarf galaxies, proving particularly efficient in erasing metallicity gradients. We propose a 'centrifugal barrier mechanism' as an alternative to the previously suggested 'fountain mechanism' for explaining the flat metallicity profiles of dIrrs and flat, rotating dEs. While only flattening the dark matter halo has little influence, the addition of angular momentum slows down the infall of gas, so that star formation (SF) and the ensuing feedback are less centrally concentrated, occurring galaxy-wide. Additionally, this leads to more continuous star formation histories by preventing large-scale oscillations in the star formation rate ('breathing'), and creates low-density holes in the interstellar medium, in agreement with observations of dIrrs.

Our general conclusion is that rotation has a significant influence on the evolution and appearance of dwarf galaxies, and we suggest angular momentum as a *second parameter* (after galaxy mass as the dominant parameter) in dwarf galaxy evolution. Angular momentum differentiates between SF modes, making our fast rotating models qualitatively resemble dIrrs, which does not seem possible without rotation.

Key words: methods: numerical – galaxies: dwarf – galaxies: evolution – galaxies: formation.

1 INTRODUCTION

Morphologically, dwarfs come in two broad classes. Early-type dwarfs, or dwarf elliptical galaxies (dEs; Ferguson & Binggeli 1994), are 'red and dead' in the sense that their stellar populations are predominantly old and that they are usually not actively forming stars. They almost completely lack the raw material for star formation (SF): gas. In a small fraction of dEs, low level central SF continues at a rate of less than $1\,M_{\odot}$ every 1000 years (De Rijcke et al. 2003a; Lisker et al. 2006). dEs with luminosities below $M_V \sim -14$ mag are usually called dwarf spheroidals, or dSphs. As a class, dEs are slowly rotating objects, flattened by velocity anisotropy (Geha, Guhathakurta & van der Marel 2003). Late-type dwarfs, or dwarf irregular galaxies (dIrrs; see e.g. Skillman 2005), are gas rich and are actively forming stars at a rate of about $1\,M_{\odot}$ every 100–1000 years. As a class, dIrrs are flattened by rotation (Côté, Carignan & Freeman 2000). Noticeably, dSphs/dEs are found predominantly in dense galactic environments while dIrrs are typically found in more sparsely populated environments. This is the so-called morphology–density relation (Binggeli, Tammann & Sandage 1987; Côté et al. 2009). In the Perseus cluster, all dwarfs, irrespective of type, appear to avoid the very dense cluster centre (Penny et al. 2009). All this suggests that the environment is at least to some extent responsible for many of the differences between dIrrs and dEs.

Despite their quite different properties, the two types of dwarfs also share many properties. They populate roughly the same mass, metallicity, luminosity, flattening (Binggeli & Popescu 1995) and size regimes and they have, to a good approximation, exponentially declining surface-brightness profiles. Moreover, the 'boundaries' between the dwarf classes are not clear-cut and transition-type objects with mixed properties exist (Grebel, Gallagher & Harbeck 2003). This body of data provides us with evidence for evolution-

★E-mail: joeri.schroyen@ugent.be (JS); sander.valcke@ugent.be (SV)
†Doctoral Fellow of the Fund for Scientific Research – Flanders, Belgium (FWO).

ary links between, or at least a 'common ancestry' for, the different types of dwarfs. As shown by e.g. Mayer et al. (2006), the combined action of ram-pressure stripping and tidal stirring on a star-forming, rotating late-type dwarf entering the halo of a Milky Way like massive galaxy can remove most of its gas and angular momentum, effectively transforming it into a quiescent, non-rotating early-type dwarf.

Dwarf galaxies entering a dense environment that are affected by ram-pressure stripping but not (or much less so) by tidal stirring would be expected to keep many of their late-type structural properties and one would expect to find dIrr/dE transition-type dwarfs. Indeed, quiescent dwarfs have been observed that are significantly more flattened and faster rotating than the average dE (De Rijcke et al. 2003b; van Zee, Skillman & Haynes 2004; Toloba et al. 2011), contain gas and dust (Conselice et al. 2003; Buyle et al. 2005; De Looze et al. 2010) and often host embedded stellar discs and spiral structures (Jerjen, Kalnajs & Binggeli 2000; Barazza, Binggeli & Jerjen 2002; De Rijcke et al. 2003b; Graham, Jerjen & Guzmán 2003).

1.1 Metallicity profiles

In general, dIrrs display chemical homogeneity practically throughout their entire stellar and gaseous bodies (Kobulnicky & Skillman 1997; Tolstoy, Hill & Tosi 2009). The Small Magellanic Cloud (SMC; Dufour & Harlow 1977; Pagel et al. 1978), NGC 6822 (Hernández-Martínez et al. 2009) and Sextans A (Kaufer et al. 2004) are examples of dIrrs without a significant chemical or abundance gradient in their gas content; the SMC (Cioni 2009) and IC 1613 (Bernard et al. 2007) also lack a stellar metallicity gradient. Thus, a flat radial metallicity profile seems to be a rather general characteristic of dIrrs. Koleva et al. (2009) present radial stellar metallicity profiles, derived from optical Very Large Telescope (VLT) spectra, of a sample of 16 dEs belonging to the Fornax cluster and to nearby groups of galaxies. They find that 10 of those, predominantly round and non-rotating, show a strong negative metallicity gradient. The six most flattened and most strongly rotating galaxies in the sample, however, show no significant gradient: like the rotationally flattened dIrrs, they are chemically homogeneous. Previous studies have also predominantly found negative metallicity gradients for dEs in the Local Group (e.g. Alard 2001; Harbeck et al. 2001, Saggitarius; – the DART project: Tolstoy et al. 2004, Sculptor; Battaglia et al. 2006, Fornax; Battaglia et al. 2011, Sextans), around M81 (Lianou, Grebel & Koch 2010) and in the Coma cluster (den Brok et al. 2011).

The findings of Koleva et al. (2009) suggest that, while total mass is most likely the dominant factor (as is concluded from the simulations of Stinson et al. 2007; Valcke, De Rijcke & Dejonghe 2008; Revaz et al. 2009; Sawala et al. 2010), angular momentum is an important second parameter in the chemical evolution of dwarf galaxies: fast rotating dwarf galaxies show a tendency to be chemically much more homogeneous than dwarfs with slow or no rotation.

An often quoted means of erasing metallicity gradients in flattened dwarf galaxies is the so-called 'fountain mechanism' (e.g. De Young & Gallagher 1990; De Young & Heckman 1994; Mac Low & Ferrara 1999; Ferrara & Tolstoy 2000; Barazza & Binggeli 2002, and references therein). The idea behind this mechanism is that the supernova feedback of a centralized SF event is capable of ejecting significant amounts of hot, enriched gas through a cavity or 'chimney' along the galaxy's minor axis. Subsequently, part of this gas can rain back down on the galaxy's disc, as in a fountain, diluting any metallicity gradient that might be present. In round low-mass galaxies, centrally concentrated supernova feedback is expected to 'blow away' *all* the gas rather than to 'blow out' only the enriched hot gas. If this fountain mechanism is correct, the absence or presence of a metallicity gradient is determined by two parameters: a dwarf galaxy's mass and its flattening or geometry.

Alternatively, due to the 'centrifugal barrier' in a rotating galaxy, gas cannot readily flow to the centre and build up a strong centrally concentrated SF event. One would therefore expect that rotation will naturally lead to more spatially extended SF and thus to more spatially homogeneous stellar populations. In a similar vein, angular momentum has been proposed in the literature as the fundamental parameter setting low angular momentum starbursting blue compact dwarfs apart from the more continuously star-forming high angular momentum dIrrs (van Zee, Salzer & Skillman 2001).

1.2 Paper

In this paper, we use a suite of new *N*-body/smoothed particle hydrodynamics (SPH) simulations to investigate how flattening affects the star formation histories (SFHs) and chemical evolution of the isolated dwarf galaxy models presented in Valcke et al. (2008). Other *N*-body/SPH simulations of similar star-forming, gas-rich dwarf galaxy models, though not always isolated, have been performed by e.g. Pelupessy, van der Werf & Icke (2004), Stinson et al. (2006), Stinson et al. (2007), Revaz et al. (2009), Governato et al. (2010), Sawala et al. (2010) and Sawala et al. (2011). We flatten our originally spherically symmetric models in different ways by adapting their initial conditions, with and without adding rotation, and compare the results both with the spherically symmetric originals and with the available observations. Our main goal is to contrast the 'fountain mechanism' with the 'centrifugal barrier' hypothesis, and to see if it is possible to produce dwarf galaxies with flat metallicity profiles in isolation.

In Section 2, we give a brief description of the simulation code, followed by a description of the simulations themselves in Section 3. We present an analysis of the simulations in Section 4, discuss the results in Section 5 and conclude in Section 6.

2 CODES

For this research, we relied mainly on two codes: the *N*-body/SPH code GADGET-2 (Springel 2005) for the simulations, and our own homemade analysis tool HYPLOT for analysing and visualizing these simulations. These will both briefly be described below.

2.1 Astrophysical mechanisms

The code we actually use for our simulations is a modified version of the *N*-body/SPH code GADGET-2 (Springel 2005). The freely available version only incorporates gravity and hydrodynamics, so to prove useful for investigating dwarf galaxy formation and evolution a number of additions were made. These include SF, feedback and radiative cooling. Re-ionization or an ultraviolet (UV) background is not included in our models. Below we give a brief overview of the implementations, more detailed information can be found in Valcke et al. (2008, 2010) and in Valcke (2010).

2.1.1 Star formation

Stars are formed when three criteria are satisfied:

$$\rho_{\rm g} \geq \rho_{\rm c} = 0.1\,{\rm cm}^{-3}, \quad (1)$$

$$T \leq T_{\rm c} = 15\,000\,{\rm K}, \tag{2}$$

$$\nabla \cdot \boldsymbol{v} \leq 0. \tag{3}$$

So we have a density threshold, a temperature threshold and the requirement that the gas be converging. We do not explicitly implement a Jeans criterion. Gas particles eligible for SF are turned into stars according to the Schmidt law (Schmidt 1959):

$$\frac{{\rm d}\rho_{\rm s}}{{\rm d}t} = -\frac{{\rm d}\rho_{\rm g}}{{\rm d}t} = c_\star \frac{\rho_{\rm g}}{t_{\rm g}}, \tag{4}$$

where $\rho_{\rm s}$, $\rho_{\rm g}$ and $c_\star$ are, respectively, the density of stars and gas, and a dimensionless SF efficiency factor. $t_{\rm g}$ is taken to be the dynamical time for the gas $1/\sqrt{4\pi G\rho_{\rm g}}$.

2.1.2 Feedback

Produced star particles are represented as 'simple stellar populations' (SSP), applying the Salpeter initial mass function (IMF) for the probability that a star of mass m resides in the SSP:

$$\Phi(m)\,{\rm d}m = Am^{-(1+x)}\,{\rm d}m, \tag{5}$$

with $x = 1.35$, $A = 0.06$, and the limits for stellar masses are $m_{\rm l} = 0.01\,{\rm M}_\odot$ and $m_{\rm u} = 60\,{\rm M}_\odot$. Feedback from a star particle is given through stellar winds (SW) and supernovae (SNe, Type II and Ia), and includes the return of both energy and enriched gas to the interstellar medium (ISM; thermal feedback). These are transferred to the surrounding gas particles according to the SPH smoothing kernel. The lower limits for SN Ia and SN II, respectively, are 3 and $8\,{\rm M}_\odot$, upper limits are 8 and $60\,{\rm M}_\odot$ and progenitor lifetimes are 5.4×10^6 and 1.5×10^9 yr.

The energy feedback for both types of SN is taken to be 10^{51} erg, for SW this is 10^{50} erg, which are all transferred to the ISM with an efficiency of 0.1.

The returned mass fractions for SN Ia and SN II are 0.00502 and 0.112, and the metal yields from these supernovae are taken from, respectively, Travaglio et al. (2004) (their b20_3d_768 model) and Tsujimoto et al. (1995). From the last authors we also adopt $N_{\rm SN\,Ia}/N_{\rm SN\,II} = 0.15$ to set the fraction of stars in the relevant mass range that reside in binary systems and that can go SN Ia. The yield M_i of element i by e.g. SN II is then calculated as

$$M_i = M_{\rm SSP}\frac{\int_{m_{\rm SN\,II,l}}^{m_{\rm SN\,II,u}} M_i(m)\Phi(m)\,{\rm d}m}{\int_{m_{\rm l}}^{m_{\rm u}} m\Phi(m)\,{\rm d}m}. \tag{6}$$

The formula for SN Ia is similar but simpler, since there is no dependence on progenitor mass ($M_i(m)$ becomes M_i).

2.1.3 Cooling

Metal-dependant gas cooling is implemented according to the cooling curves from Sutherland & Dopita (1993). These curves are interpolated in metallicity and temperature to obtain the cooling strength for a gas particle. They are allowed to cool in this fashion to a minimum of 10^4 K, below which further cooling is only possible through adiabatic expansion.

2.2 Analysis and visualization

For the analysis we used our own HYPLOT package, which is freely available on SourceForge.[1] It is an analysis/visualization tool specially suited for *N*-body/SPH simulations (currently only specifically for GADGET-2 data files), written mainly in PYTHON and C++. PYQT and MATPLOTLIB are used for the GUI and the plotting, and it is also fully scriptable in PYTHON. All analysis, plots and visualizations in this paper have been made using HYPLOT.

[1] http://sourceforge.net/projects/hyplot/

Table 1. Details of the basic spherical dwarf galaxy models (see Valcke et al. 2008). Initial masses for the DM halo and gas are in units of $10^6\,{\rm M}_\odot$, radius in kpc.

Model	$M_{\rm DM,i}$	$M_{\rm g,i}$	a_0
C01	206	44	0.439
C03	330	70	0.513
C05	660	140	0.646
C07	1238	262	0.797
C09	2476	524	1.004

3 SIMULATIONS

In this section we will describe the simulations themselves: the models used for the basic initial conditions, the additional set-up we need for our goals and finally the grid of our production runs, together with a preliminary evaluation of those runs to have an idea of the simulated objects we have at our disposal.

3.1 Initial conditions

We base the initial conditions of our flattened dwarf galaxy simulations on the spherically symmetric dwarf galaxy models of Valcke et al. (2008). We describe these briefly below and in Table 1. We introduce flattening into the models by adding initial flattening and/or rotation. The precise way in which this is done is described below. In the end, we have a set of flattened dwarf galaxies, both rotating and non-rotating. This way, we can distinguish between the effects of the *geometry* (flattening only) and the *kinematics* (i.e. rotation).

3.1.1 Spherically symmetric dwarf galaxy models

The basic spherically symmetric dwarf galaxy models come from Valcke et al. (2008). They consist of

(i) a dark matter halo with a cored *Kuz'min Kutuzov* density profile (Dejonghe & de Zeeuw 1988);

(ii) a spherically symmetric homogeneous gas cloud, set to a fixed initial temperature of 10^4 K, initial metallicity of $10^{-4}\,{\rm Z}_\odot$ and the gas particles initially at rest.

We start off with only gas and dark matter (DM). The gas cools and collapses into the DM gravitational potential well. Our modified version of GADGET-2, as described in the previous section, then allows the gas particles to produce star particles if the criteria are satisfied (of which the density criterion proves to be the most important). Feedback of energy and of newly synthesized elements from these star particles is accounted for. For specific information and details on these models, we refer to Table 1 and Valcke et al. (2008). The actual initial condition files are created by random (Poisson) sampling of these density profiles for both components.

3.1.2 Adding initial rotation

Rotation is added *to the gas only* in the initial conditions. The DM halo, implemented as a live halo, simply provides a background gravitational potential and is not given any rotation. Every gas particle is given a tangential velocity according to the desired rotation profile. We align the z-axis with the galaxy's rotation axis.

Our preferred rotation profile is a *constant radial rotation profile* (CR), which means that the net velocity given to each gas particle is independent of radius. We do not use a *solid body rotation profile* (SBR), in which the velocity depends linearly on the radial distance from the rotation axis. This is because preliminary tests showed that using SBR, a significant fraction of the gas content of the galaxy immediately became unbound and was lost, even at low rotation speeds. The CR profile we use can be argued to have problems on small radii. The constant value of the velocity means that the angular velocity rises quickly when approaching the rotation axis. But here our preliminary tests show that in practice this is not a problem. Because the gas particles are placed randomly and we are working with floating point numbers, no particle in practice will ever lie exactly on the rotation axis. The gas particles in the central region initially have a very high angular velocity, but interactions between the gas particles quickly slow them down and convert the excess velocity to heat, which is then very quickly lost through the very efficient radiative cooling. Furthermore, since the gas is initially distributed homogeneously over a large sphere, there is no large gas mass in this central region. We did a number of test simulations with a variety of alternative rotation profiles with more well behaved central velocities:

(i) the rotation velocity rises as an arctangent with radius, with the asymptotic velocity equal to the constant value of the fiducial models;

(ii) the rotation velocity rises linearly out to 0.5 kpc and is then kept constant at the constant value of the fiducial models ('combined linear/constant');

(iii) the rotation velocity rises as an arctangent with radius out to 0.5 kpc and is then kept constant at the constant value of the fiducial models ('combined arctangent/constant').

These simulations show no noticeable influence of the central velocity profile on the behaviour of the models, see Fig. 1.

We will henceforth refer to the set of CR models as the 'rotating models'.

3.1.3 Adding initial flattening

As a flattening parameter we consistently use the axial ratio $q = c/a$ in this paper, where c is the shortened z-axis and a is the axis in the x–y plane (we adopt axially symmetric models). Here, we flatten both the gas and DM distributions. The parameters of the Kuz'min Kutuzov profile naturally allow for introducing a flattening to the DM halo in the form of an axial ratio (Dejonghe & de Zeeuw 1988), so the DM part of the flattening is trivial. Flattening the homogeneous gas sphere takes a little bit more care. We need to scale up the axis in the x–y plane appropriately while scaling down the z-axis to ensure that the density of the gas cloud remains the same. This is important because we do not want to change any aspect of the dwarf galaxy models from Valcke et al. (2008), other than the geometry, and the initial density is a very important one. Starting from a sphere with radius r, if we want to achieve a flattening q we produce it by calculating the a and c axes as follows:

$$a = rq^{-1/3},$$
$$c = rq^{2/3}.$$

This will ensure that the volume of the ellipsoid is constant for any value of q, and therefore so is the density.

In the remainder, we will refer to this set of models as the 'flattened models' (although of course the rotating models also become flattened eventually).

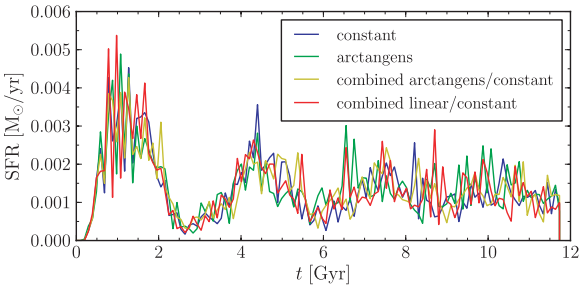

Figure 1. The SFR as a function of time for four different rotation profiles (see text for details).

3.2 Production runs

In Table 2 we show an overview of the run numbers and specifications of our production runs. We simulate dwarf galaxies with a range of masses, flattenings and rotation speeds using the dwarf galaxy models of Valcke et al. (2008) from Table 1 and additional methods for setting up the initial conditions as described above. Both the gas and the dark matter components were represented by 200 000 particles, and the simulations were evolved in time during 11.7 Gyr, corresponding to the time from $z = 4.3$ to the present. The seeds used for sampling the particles from the specified density profiles (see Section 3.1.1) are chosen at random for all production runs.

Table 2. Grid of the production runs, given with run numbers and specifications of the three used parameters: mass (first column, see Table 1), initial flattening (q, last column) and initial rotation speed (v_i, three different rotation speeds).

DG model				q
	0 km s^{-1}	1 km s^{-1}	5 km s^{-1}	
C01	201	211	221	1
	231	241	251	0.5
	261	271	281	0.1
C03	203	213	223	1
	233	243	253	0.5
	263	273	283	0.1
C05	205	215	225	1
	235	245	255	0.5
	265	275	285	0.1
C07	207	217	227	1
	237	247	257	0.5
	267	277	287	0.1
C09	209	219	229	1
	239	249	259	0.5
	269	279	289	0.1

Table 3. Details of simulations. All physical quantities are evaluated at the end of the simulation (11.7 Gyr), except those indexed with 'i', which are evaluated at the beginning. Columns: (1) model number (see Table 1), (2) simulation number, (3) initial flattening (gas/DM), (4) initial rotation speed of gas ($\mathrm{km\,s^{-1}}$), (5) spin parameter of gas in IC, (6) final gas mass ($10^6\,\mathrm{M_\odot}$), (7) stellar mass ($10^6\,\mathrm{M_\odot}$), (8) half-light radius (kpc), (9)–(10) *B*- and *V*-band magnitude, (11)–(12) fitted Sérsic parameters of surface brightness profile, (13) central stellar velocity dispersion along line of sight (edge-on) ($\mathrm{km\,s^{-1}}$), (14)–(15) luminosity-weighted metallicity (*B* band), (16) final flattening of the stellar component (averaged over last 3 Gyr), (17) final stellar peak rotation speed ($\mathrm{km\,s^{-1}}$). Omitted values were irrelevant due to low stellar mass.

Model (1)	Run (2)	q_i (3)	v_i (4)	λ (5)	$M_\mathrm{g,f}$ (6)	$M_\star$ (7)	R_e (8)	M_B (9)	M_V (10)	I_0 (11)	n (12)	$\sigma_\mathrm{1D,c}$ (13)	$Z\,(\mathrm{Z_\odot})$ (14)	[Fe/H] (15)	q_f (16)	v_f (17)
C01	201	1	0	0.0	43.5	0.485	0.18	−7.84	−8.44	26.3	0.81	8.9	0.00036	−1.907	0.99	0.7
	211	1	1	0.007	43.5	0.519	0.15	−8.23	−8.76	26.5	0.62	8.2	0.00169	−1.088	1.0	3.0
	221	1	5	0.036	43.8	0.235	0.13	−7.89	−8.39	27.0	0.35	6.5	0.00247	−1.005	0.96	2.9
	231	0.5	0	0.0	43.6	0.373	0.17	−7.83	−8.37	26.4	0.8	7.7	0.00113	−1.241	0.74	1.0
	241	0.5	1	0.009	43.6	0.419	0.17	−7.91	−8.51	26.3	0.78	7.3	0.0016	−1.109	0.72	5.8
	251	0.5	5	0.046	43.9	0.138	0.13	−7.65	−8.08	26.5	0.57	5.8	0.00188	−1.106	0.69	1.9
	261	0.1	0	0.0	44.0	0.008	0.11	−3.57	−4.19	–	–	5.6	0.00073	−1.561	–	−0.1
	271	0.1	1	0.014	44.0	0.004	0.11	−2.65	−3.25	–	–	4.6	0.00021	−2.03	–	–
	281	0.1	5	0.071	44.0	0.0	–	–	–	–	–	–	–	–	–	–
C03	203	1	0	0.0	67.6	2.316	0.22	−9.8	−10.34	25.2	0.68	12.1	0.00187	−1.103	1.02	1.4
	213	1	1	0.008	67.9	2.101	0.22	−9.77	−10.3	25.3	0.68	12.0	0.00219	−1.058	0.93	4.9
	223	1	5	0.039	68.3	1.671	0.25	−9.84	−10.36	25.2	0.59	10.7	0.00368	−0.825	0.76	13.7
	233	0.5	0	0.0	67.7	2.283	0.25	−9.65	−10.25	25.9	0.55	11.3	0.00163	−1.095	0.75	1.0
	243	0.5	1	0.01	67.6	2.354	0.28	−9.94	−10.49	24.8	0.72	11.2	0.00371	−0.795	0.7	8.2
	253	0.5	5	0.05	68.6	1.377	0.26	−9.69	−10.21	25.4	0.56	10.0	0.00373	−0.826	0.61	12.9
	263	0.1	0	0.0	69.3	0.691	0.19	−8.88	−9.39	24.5	0.92	9.2	0.00256	−0.964	0.64	0.7
	273	0.1	1	0.015	69.3	0.68	0.19	−8.75	−9.3	24.7	0.98	9.5	0.00262	−0.97	0.6	4.1
	283	0.1	5	0.076	69.7	0.293	0.15	−8.32	−8.78	24.8	0.85	8.3	0.00284	−0.958	0.57	3.0
C05	205	1	0	0.0	122.2	17.538	0.39	−11.84	−12.48	24.2	0.62	19.5	0.00445	−0.699	1.0	0.4
	215	1	1	0.009	114.1	25.561	0.45	−12.1	−12.79	24.4	0.59	20.9	0.00513	−0.674	0.94	9.3
	225	1	5	0.043	123.3	16.562	0.63	−12.37	−12.86	24.5	0.5	14.4	0.00623	−0.61	0.53	24.2
	235	0.5	0	0.0	128.3	11.496	0.35	−11.54	−12.12	24.1	0.66	16.1	0.00291	−0.886	1.03	1.2
	245	0.5	1	0.011	111.2	28.514	0.59	−12.76	−13.3	24.5	0.36	20.4	0.00822	−0.484	0.72	14.4
	255	0.5	5	0.056	126.4	13.42	0.65	−12.14	−12.65	25.2	0.38	12.6	0.0063	−0.609	0.45	24.2
	265	0.1	0	0.0	133.4	6.491	0.38	−11.18	−11.71	24.9	0.47	16.4	0.00305	−0.871	0.67	−0.3
	275	0.1	1	0.017	129.5	10.351	0.47	−11.87	−12.38	24.8	0.43	16.5	0.0052	−0.69	0.63	8.7
	285	0.1	5	0.086	136.3	3.633	0.42	−10.96	−11.43	25.3	0.45	15.2	0.00436	−0.771	0.49	11.7
C07	207	1	0	0.0	84.9	175.6	0.55	−14.21	−14.92	22.8	0.67	32.8	0.01396	−0.241	1.0	4.4
	217	1	1	0.01	88.1	172.35	0.57	−14.16	−14.86	22.6	0.71	31.0	0.01525	−0.191	0.88	18.6
	227	1	5	0.048	173.6	87.62	1.09	−14.0	−14.53	24.6	0.39	18.5	0.00836	−0.478	0.45	33.6
	237	0.5	0	0.0	144.9	115.46	0.7	−14.09	−14.7	23.5	0.48	32.1	0.01103	−0.355	0.89	2.4
	247	0.5	1	0.012	110.1	150.53	0.69	−14.27	−14.9	23.2	0.58	29.0	0.01346	−0.257	0.73	18.5
	257	0.5	5	0.062	197.8	63.68	1.17	−13.51	−14.09	25.2	0.38	16.5	0.00631	−0.609	0.38	34.4
	267	0.1	0	0.0	195.6	65.82	0.81	−13.95	−14.45	24.1	0.41	26.6	0.00853	−0.482	0.76	1.6
	277	0.1	1	0.019	194.0	67.354	0.82	−13.98	−14.46	24.2	0.36	28.1	0.00892	−0.455	0.68	8.5
	287	0.1	5	0.095	240.6	21.168	0.84	−12.91	−13.37	25.0	0.38	18.2	0.00595	−0.642	0.39	25.3
C09	209	1	0	0.0	44.0	475.84	0.33	−14.79	−15.56	20.4	1.29	43.0	0.01594	−0.109	1.02	2.7
	219	1	1	0.011	46.7	473.57	0.48	−14.8	−15.58	21.0	1.11	40.3	0.01591	−0.135	0.83	28.4
	229	1	5	0.054	177.0	344.39	1.34	−15.12	−15.71	23.8	0.51	24.1	0.01363	−0.238	0.4	45.3
	239	0.5	0	0.0	61.5	458.48	0.43	−14.84	−15.6	20.9	1.12	42.7	0.0167	−0.104	0.83	2.0
	249	0.5	1	0.014	67.8	452.32	0.58	−14.86	−15.63	21.8	0.89	37.3	0.01634	−0.129	0.69	29.6
	259	0.5	5	0.07	238.4	283.58	1.52	−14.9	−15.5	24.1	0.61	21.2	0.01078	−0.348	0.36	44.5
	269	0.1	0	0.0	211.0	310.25	0.61	−15.28	−15.82	21.6	0.75	36.0	0.01835	−0.086	0.79	0.4
	279	0.1	1	0.021	225.5	295.97	0.74	−15.18	−15.74	22.5	0.58	35.6	0.01663	−0.137	0.72	14.2
	289	0.1	5	0.107	410.0	113.12	1.19	−14.36	−14.89	23.7	0.9	27.2	0.00812	−0.491	0.39	29.7

3.3 Preliminary evaluation of simulations

Table 3 lists many different physical quantities for all of the simulated dwarf galaxies in our set from Table 2. These are the final values for these quantities, evaluated at the end of the simulation, except those explicitly indexed with 'i', which are initial values. Broad-band colours are calculated (with bilinear interpolation) using the models of Vazdekis et al. (1996), who provide mass/luminosity

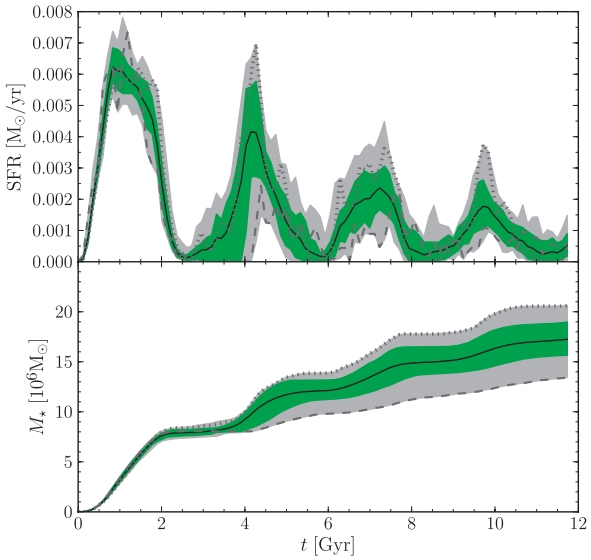

Figure 2. Depiction of the variance inherent to our models, using a set of 25 differently sampled initial conditions. Upper panel shows the evolution of the SFR. Lower panel shows the evolution of the total stellar mass. The black line is the mean curve for our set. The green band shows the area between the 15.9th and 84.1st percentile (which are linearly interpolated between the closest ranks, and would correspond to the 1σ interval if the underlying distribution was Gaussian), and the light grey band shows the area between the minimum and maximum value of our set. These percentiles and extrema are calculated in each time-bin (of which there are 100). The two dark grey lines show the evolution of two individual runs: the dashed and dotted line represent the runs which, respectively, produced the lowest and the highest total stellar mass at the end of the simulation.

values for SSPs according to metallicity and age. For those simulations that form little or no stars, making an accurate evaluation of the physical parameters impossible, we simply enter a '−' in Table 3.

To evaluate our methods for setting up the initial conditions, we discuss the C05 models below (see Table 2).

3.3.1 *Variance*

We first make note of the inherent variance in our models. To this end we have produced a set of 25 simulations of the basic spherical C05 model, with different samplings of the dark matter halo and the gas sphere. For each simulation, different random seeds are used to construct the initial condition. As shown by the 15.9th/84.1th percentile area and the total range of the SFHs of this set of simulations in Fig. 2, the variance is significant, allowing for a variety of SFHs. This is however not unexpected. Systems of this kind, with stochastic SF and feedback, are inherently chaotic. Small differences are continuously amplified and can, over time, lead to large deviations. However, on the other hand, more importantly, the green band depicting the 15.9th/84.1th percentile area (which would correspond to the 1σ interval if the underlying distribution was Gaussian) shows quite clearly the generic behaviour of the models. So we keep in mind that our models can show a spread in their properties, but that they also exhibit a clear general behaviour.

3.3.2 *Rotating models*

As described above, to obtain a rotating galaxy we add initial angular momentum to the *gas*. We need to check if this actually results in a rotating *stellar* component of the galaxy. In the upper panel of Fig. 3, we present the rotation curve of the gas particles at different times. In the lower panel, we show the final stellar rotation curve (at 11.7 Gyr). These are binned profiles of tangential velocity versus distance to the z-axis, where the profile value in every bin is the average rotation velocity per particle in that bin.

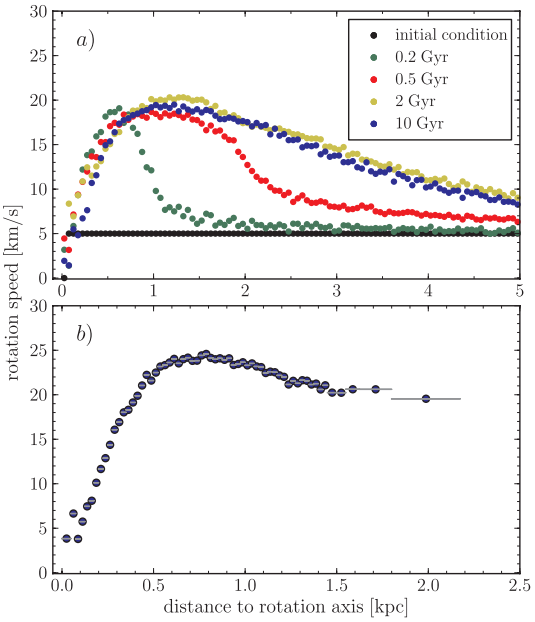

Figure 3. Rotation curves of our showcase model (225), upper panel displays the gas at different times during the simulation, lower panel displays the stars at 11.7 Gyr (with adaptive binning).

The rotation profile of the gas rises due to the gas falling into the potential well, and quickly evolves to a rather stable form, only perturbed temporarily by the turbulence caused by strong SF events. This 'steady state' is a consequence of the balance between cooling, which makes the rotating gas sink inwards, and supernova feedback, which heats and disperses gas. The stars that form from the gas finally follow a rotation profile that rises out to one half-light radius and flattens off beyond that radius. This confirms that using CR initial conditions for the gas is adequate to achieve stable, rotating dwarf galaxies. The final rotation speed of the stars which is included in Table 3 is the peak value of this rotation curve.

3.3.3 *Flattened models*

In Fig. 4 we show three of our model galaxies (a non-rotating spherically symmetric model on the left, a rotating model and a flattened model) to see the resulting flattenings at the end of the simulations. The latter two both show a considerable and stable flattening (see the C05 model in Fig. 5). Some trends become apparent when looking at the total mass range in Table 3 and Fig. 5. It appears that the stability of q for the stellar component significantly increases with rising mass in the rotating models. Only in the least massive models does q rise significantly with time. The more massive models all exhibit a stable flattening around $q \sim 0.4$–0.5, so our model dwarf galaxies are relatively 'thick'. In non-rotating models with an initially strongly flattened halo, the halo thickens and it turns out to be impossible to make stellar bodies more flattened than $q \sim 0.6$–0.8. As can be read from Table 3, combining initial rotation and initial flattening helps somewhat to achieve stronger flattenings in the least massive models.

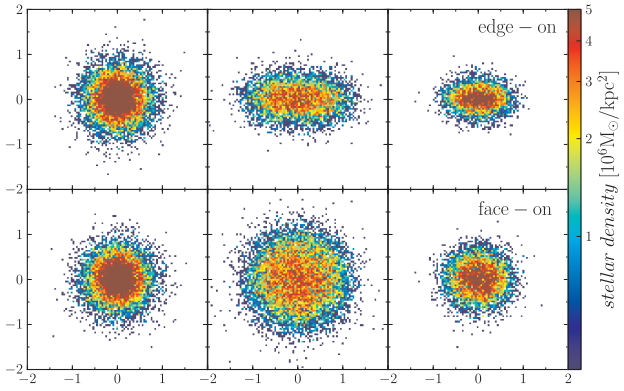

Figure 4. Edge-on and face-on views of the stellar distributions of a non-rotating spherical model (left, 205), a rotating model (middle, 225) and a flattened, non-rotating model (right, 265). All are slices of thickness 0.4 kpc, axes are in kpc and colour denotes projected stellar density.

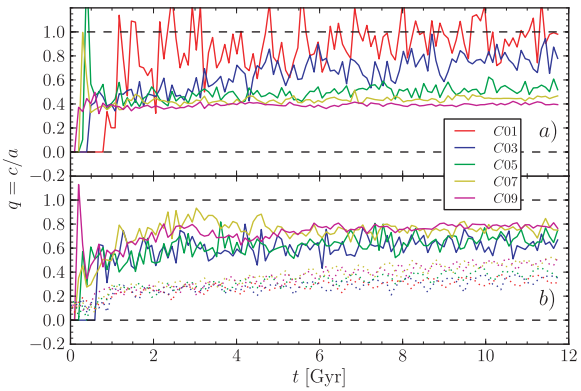

Figure 5. Evolution of the flattening parameter $q = c/a$ of the stellar component during the simulations for different galaxy masses. Upper panel: rotating models (all with $v_i = 5\,\mathrm{km\,s^{-1}}$); lower panel: flattened models (all with $q_i = 0.1$). Per panel all properties are identical, except for the mass. Only galaxies with an appreciable stellar mass are shown (see Table 3). Dotted lines show the q of the DM component, only shown in the bottom panel because the DM consistently has $q = 1$ in the top panel.

We thus note from Table 3 and Fig. 5 that we are not able to make extremely flat galaxies. In the work of Roychowdhury et al. (2010) a collection of dIrrs from the Faint Irregular Galaxies GMRT Survey (FIGGS) is investigated, and they find from the flattening distribution a mean axial ratio $\langle q \rangle \approx 0.6$ for the *H I discs*. Similar values are obtained by Binggeli & Popescu (1995), Staveley-Smith, Davies & Kinman (1992), Hunter & Elmegreen (2006), Sung et al. (1998) and Sánchez-Janssen, Méndez-Abreu & Aguerri (2010) for the *stellar* content of dwarf galaxies. Also other simulations suggest that low-mass galaxies are not born as thin discs, but as thick, puffy systems [e.g. Kaufmann, Wheeler & Bullock 2007; and to a lesser extent the (more massive) models of Governato et al. 2010, which are still not extremely flat]. The reason for this is sought in the increasing importance of turbulent motions, plausibly caused by SF and feedback, with respect to rotational motion in low-mass systems (Kaufmann et al. 2007; Roychowdhury et al. 2010; Sánchez-Janssen et al. 2010). Besides the moderate value of the flattening itself, we also qualitatively reproduce the trend with galaxy mass from Sánchez-Janssen et al. (2010). All our simulations are below their 'limiting mass' of $M_* \approx 2 \times 10^9\,\mathrm{M_\odot}$, and indeed for simulations with identical initial set-up, the final stellar bodies thicken with decreasing mass. This can be seen in Fig. 6, where we mimic their

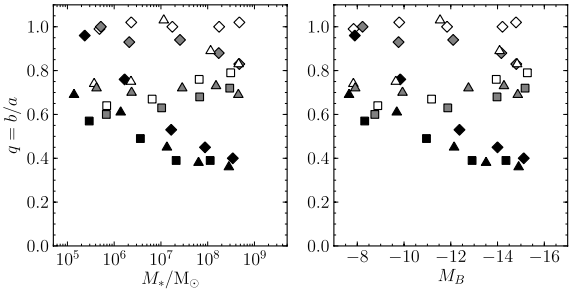

Figure 6. Axis ratios of all our models. Left-hand panel: versus stellar mass (in $\mathrm{M_\odot}$); right-hand panel: versus B-band luminosity. The different initial rotation speeds are indicated with colour (white: $0\,\mathrm{km\,s^{-1}}$; grey: $1\,\mathrm{km\,s^{-1}}$; black: $5\,\mathrm{km\,s^{-1}}$), the initial flattenings are indicated with symbol shapes (lozenge: 1; triangle: 0.5; square: 0.1).

fig. 1 (the leftmost and rightmost panels). Our most massive, flat models ($M_* \approx 3.4 \times 10^8\,\mathrm{M_\odot}, q \approx 0.4$) connect nicely to models DG1 and DG2 of Governato et al. (2010), who are slightly more massive and slightly flatter ($M_* \approx 4.8 \times 10^8\,\mathrm{M_\odot}, q \approx 0.35$).

3.3.4 Galaxy mass and concentration

For a rotating model the half-light radius (R_{eL}), defined as the radius of the sphere containing half of the light, is considerably larger than that of a spherical model, as can be seen in Table 3 and Fig. 4. The total stellar mass usually decreases when adding significant rotation. Non-rotating flattened models on the other hand are generally not much larger than the spherical models, sometimes even smaller. The half-light radius decreases slightly in flattened galaxies at lower masses, and increases slightly at higher masses (with respect to the spherical model). The total stellar mass decreases with increasing flattening.

The rotating models are thus spatially more extended than their spherical progenitor and at the same time they generally are also less massive (in stellar mass) so they are considerably less centrally concentrated. The flattened, non-rotating models are usually less spatially extended than the spherical models and also less massive, so they have similar central concentrations (see also Fig. 4).

4 ANALYSIS

In this section we present a more extensive analysis of our production runs.

4.1 Metallicity profiles

Looking at Fig. 7 we see some interesting results concerning the metallicity profiles of the rotating galaxies. For a range of galaxy masses we compare the metallicity profiles of the spherical models with those of the fastest rotating models from Table 2 (with $v_i = 5\,\mathrm{km\,s^{-1}}$) in Fig. 7. The metallicity profiles of the spherical models almost always show a clear, negative gradient, while the profiles of the rotating models are always significantly flatter. For a proper comparison between different models of different sizes, the half-light radius of each simulation is also indicated on the plots with a dashed vertical line. We note that the rotating models can be considered to have flat profiles out to 1.5 times R_{eL}, while the spherical models usually show a fall-off well before that. Noticeably, the mean [Fe/H] of the lower mass models appears to be significantly

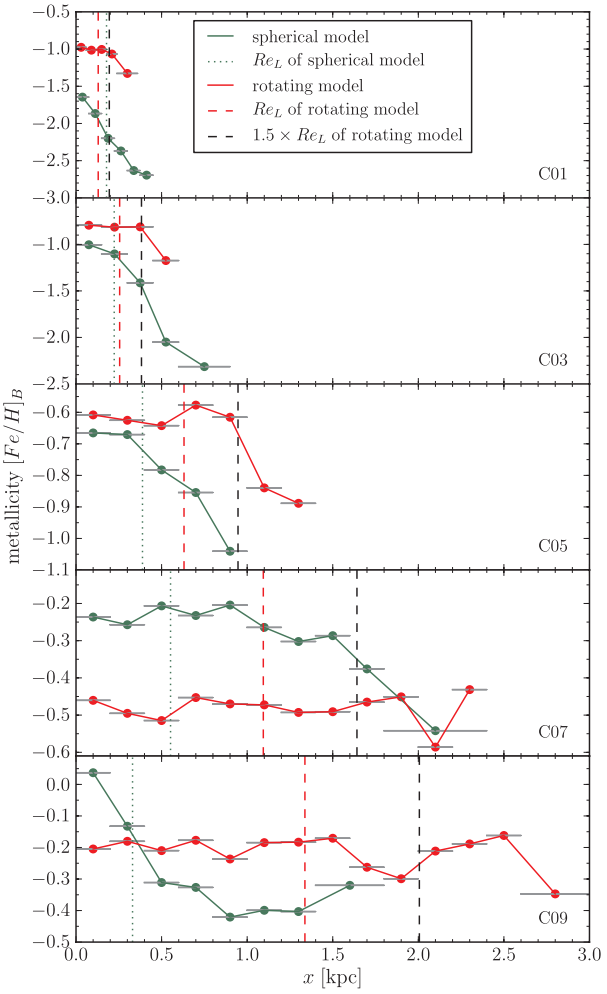

Figure 7. Metallicity profiles of our productions runs, see Table 2. Each frame compares, for a certain galaxy mass, the spherical model (20*x*) with the fastest rotating model (22*x*). The R_{eL} of each model is also indicated with a dashed line, and for the rotating model we also show $1.5R_{eL}$ for indicative purposes. Adaptive binning was used to produce these profiles, the width of each bin being indicated by a horizontal grey bar.

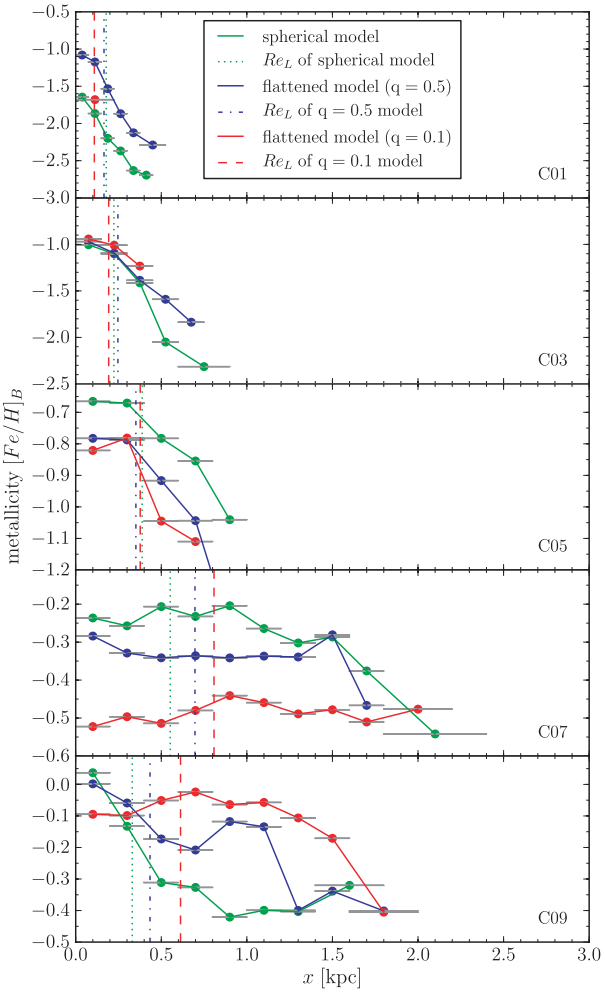

Figure 8. Metallicity profiles of our productions runs, see Table 2. Each frame compares, for a certain galaxy mass, the spherical model (20*x*) with the two non-rotating flattened models (23*x* and 26*x*). Further details of the plot are similar to those of Fig. 7.

higher when rotating, while the opposite is true for the higher mass models. This will be discussed further on in Section 4.4.4.

Fig. 8 shows the same quantities for some of the flattened models. Surprisingly, there appears to be no obvious trend between the flattening and the shape of the metallicity profile, with most galaxies showing strong negative metallicity gradients. We show all models from Table 2 which received an initial flattening but no initial rotation, so for each mass we have two different degrees of initial flattening ($q = 0.5$ and 0.1). It is clear that the flattening generally has no significant effect on the metallicity gradient, almost all simulations have a negative slope. Only in the most massive ones, or where the spherical model does not have a strong gradient to begin with, does the initial flattening appear to have some ability to somewhat flatten the metallicity profile.

4.2 Star formation histories

Next we turn our attention to the SF, and for this we look at Fig. 9, where SFHs of different simulations are shown. Rotation also seems to have a significant influence here. We again compare the spherical models with the fastest rotating models from Table 2 for a range of galaxy masses in Fig. 9, where we show the evolution of the produced stellar mass expressed in solar mass per year ($M_\odot$ yr^{-1}). The total stellar mass of the galaxy is plotted in dashed lines alongside the SFHs.

Non-rotating spherical models typically have 'breathing' or 'bursty' SFHs, with strong SF peaks a few Gyr long, separated by quiescent periods where the star formation rate (SFR) essentially goes to zero (Stinson et al. 2007; Valcke et al. 2008; Revaz et al. 2009). The strength and duration of these peaks, as well as the intermittent pauses, depend mainly on galaxy mass.

The models with rotation, however, are able to reduce this burstiness and make the SFH much more continuous. Periods of increased SF still exist, alternated with lulls, but the SFR never drops down to zero. The effectiveness of reducing the SF peaks varies in our simulations, and depends primarily on the galaxy mass. In the least massive models, which in the non-rotating spherical case show the most extreme bursty behaviour (one big initial burst almost completely shutting down further SF activity), the effect of adding rotation is most noticeable. The SFR now becomes virtually flat. The more massive models still show some SF fluctuations but not nearly as pronounced as in their spherically symmetric analogues.

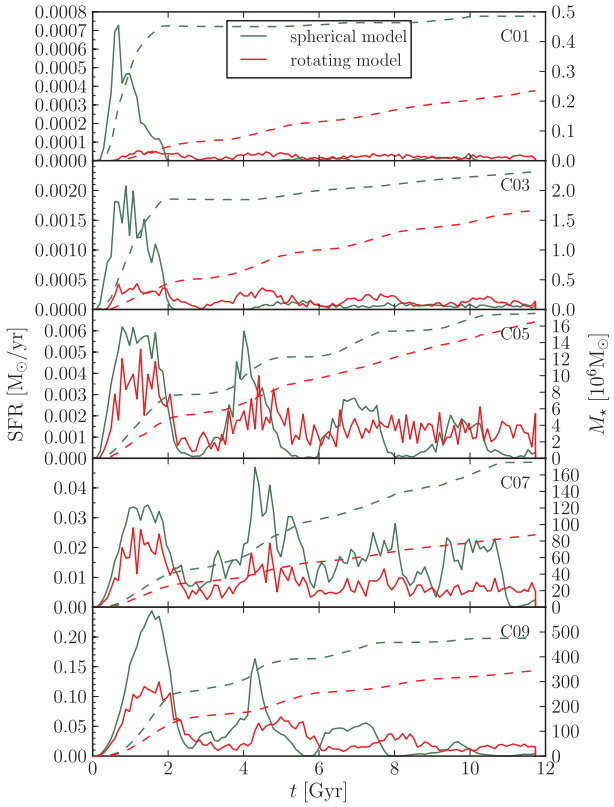

Figure 9. SFHs of our productions runs, see Table 2. The same runs as in Fig. 7 are plotted here, comparing spherical and rotating models for different masses. Both their SFH (solid lines) and evolution of their stellar mass (dashed lines) are shown.

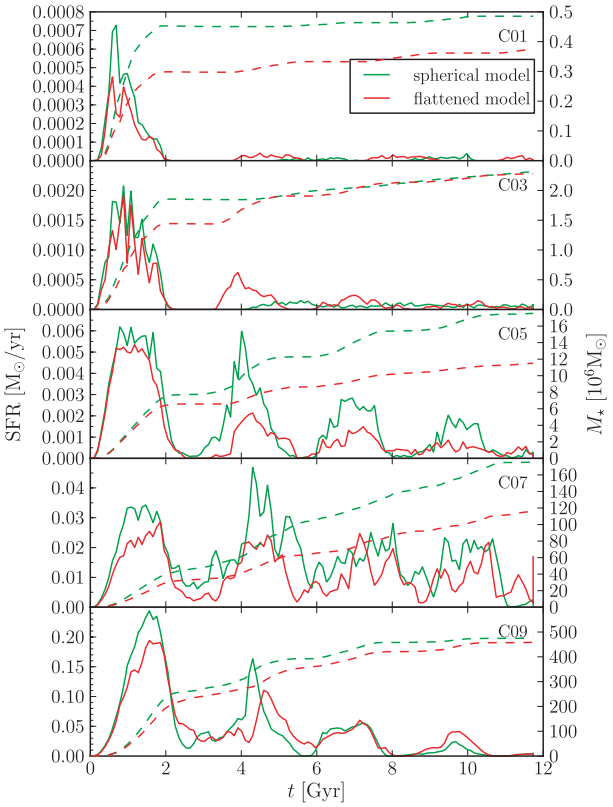

Figure 10. SFHs of our productions runs, see Table 2. The runs with $q = 0.5$ from Fig. 8 are plotted here, comparing spherical and flattened models for different masses. Similar to Fig. 9.

Flattening on the other hand does not have a large effect on the SFH of the galaxies. When looking at Fig. 10 we can see that flattening, unlike rotation, generally does not induce major qualitative differences in the SFH. The SFHs are generally very much like the SFHs of the spherical models, still having large peaks separated by periods with zero SF.

4.3 Gas structure

The structure of the gas of dwarf galaxies is another typical characteristic that we will consider. The best observations available in this respect come from the Magellanic Clouds; for instance Kim et al. (2005) present H I data for the LMC. Another very useful source of observational data about the H I gas content and structure of dwarf galaxies is The H I Nearby Galaxy Survey (THINGS; Walter et al. 2008; Weisz et al. 2009). These studies show that the neutral hydrogen gas of dIrrs generally shows an obvious 'bubble structure', consisting of myriad spherical low-density regions or 'holes' in the gas with a large range of sizes.

The origin of these holes has long been attributed to stellar feedback by single-age newborn stellar clusters (Weaver et al. 1977; McCray & Kafatos 1987, and references therein). However, for the LMC it has proven to be not at all evident to correlate H I holes or shells with Hα emission (Kim et al. 1999; Book, Chu & Gruendl 2008). Holmberg II has similar issues, with Hα not tracing the holes, and the stellar ages found therein not corresponding well with the kinematical age of the holes (Rhode et al. 1999; Stewart et al. 2000; Weisz et al. 2009). Studying this last galaxy in detail, Weisz et al. (2009) propose a multi-age model, where H I holes are created by stellar feedback from multiple generations of SF spread out over tens to hundreds of Myr. This model is supported by the fact that Hα and 24-μm emission, which trace the most recent SF, do not correlate well with H I holes, while UV emission, which traces SF over roughly the last 100 Myr, correlates much better. The concept of a single age for a hole is rendered ambiguous.

In Fig. 11 we show the structure of three of our simulated dwarf galaxies, in a sequence of snapshots taken throughout their entire evolution (all shown face on). The projected gas density is rendered as the background colour (see colour bar), and two different age selections of the stellar population are plotted. In accordance with Weisz et al. (2009) we choose these to represent the *newest* stars (yellow dots, stellar age <20 Myr) which would be detected in Hα, and the *recent* stars (red dots, 40 Myr < stellar age < 100 Myr) which would show up in UV. The gap between the two populations serves to provide a clearer distinction between them on the plots. These three simulations compare a spherical model (205, left-hand column), a flattened non-rotating model (265, right-hand column) and a rotating model (225, centre column), all based on the C05 model (see Tables 1 and 2). The specific snapshot times have been selected to represent 'interesting' moments in the galaxies' SFHs, coinciding with SF peaks or lulls, see Figs 9 and 10. A full, high-quality animation, corresponding to Fig. 11, can be found online.[2]

[2] HD video: http://www.youtube.com/watch?v = L2OWqfM1azo
YouTube channel of the Astronomy department at Ghent University: http://www.youtube.com/user/AstroUGent
YouTube playlist with all additional video material for this paper: http://www.youtube.com/user/AstroUGent#g/c/EFAA5AAE5C5E474D

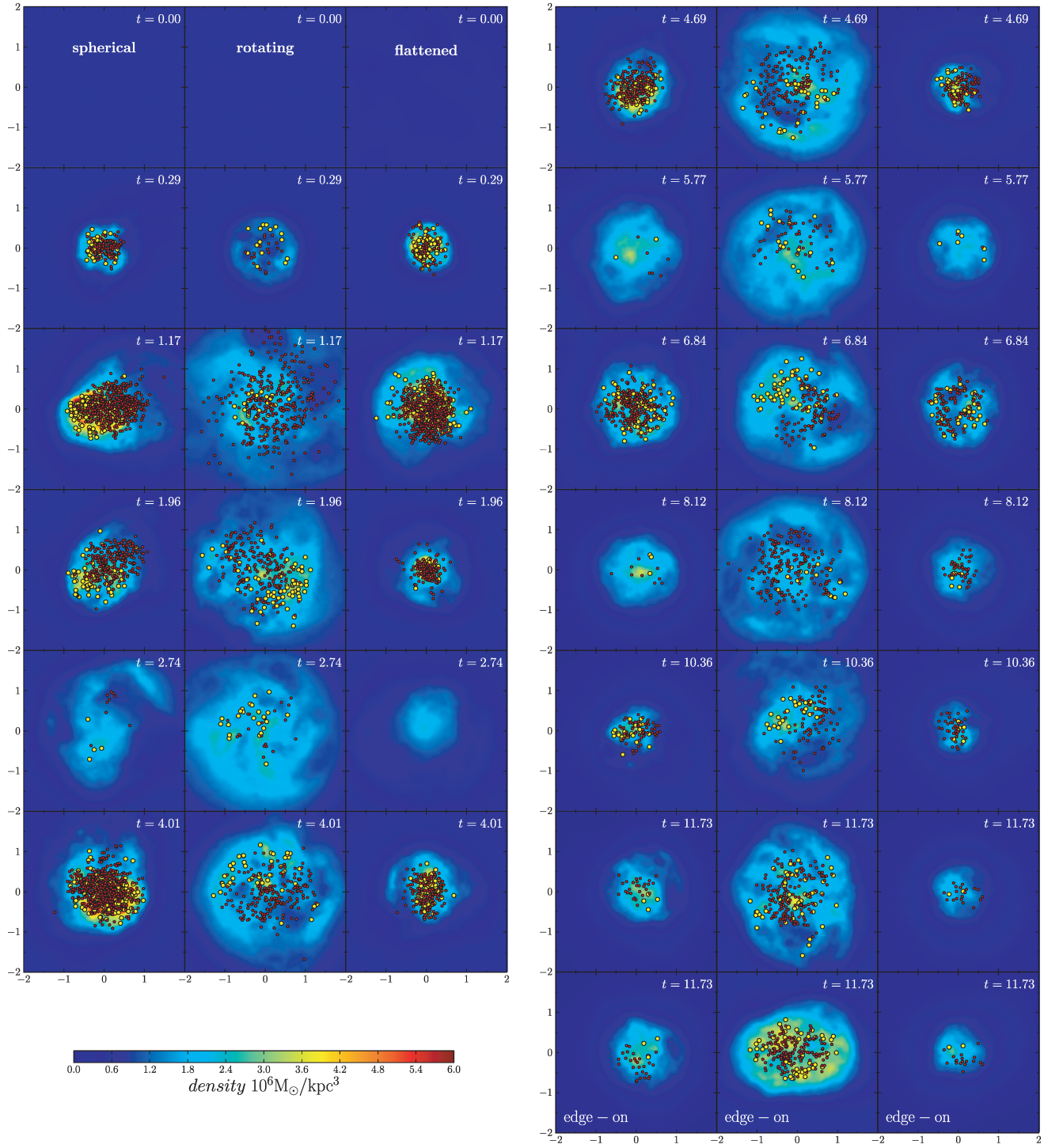

Figure 11. A series of snapshots from the evolution of three simulated dwarf galaxies based on the C05 DG model. Left-hand column: basic spherical model (205); middle column: rotating model (225); right-hand column: flattened, non-rotating model (265). The bottom of the left three columns continues on the top of the right three columns. Snapshots show rendered gas density (colour bar), *new* star particles (yellow dots, stellar age <20 Myr) and *recent* star particles (red dots, 40 Myr < stellar age < 100 Myr). The label in the top right-hand corner indicates the time in the simulation (Gyr), and all galaxies are shown face-on in the *x*–*y* plane, except the last three snapshots which are edge-on in the *x*–*z* plane (axes are in kpc). A full, high-quality animation can be found online and as Supporting Information with this article – see text.

4.3.1 Spherical simulations

In the spherical models gas collapses to the centre and forms stars that collectively blow out the gas through feedback, preferably to one side in a so-called chimney (see snapshots at $t = 1.17$). Over time, the gas cools and recollapses after which SF can resume again (snapshots at $t = 2.74$, 5.77 and 8.12). This cycle continues throughout the entire evolution. There is no significant

difference in the correlation with the local gas density between the two stellar populations shown in Fig. 11. Both populations are centrally concentrated, and so is the gas density.

Overall there is little small-scale structure: the behaviour of the gas takes place on a large, collective scale. This becomes particularly apparent when comparing to the rotating model, discussed further on in Section 4.3.3. An occasional small bubble can be spotted in the gas when the galaxy is forming stars (e.g. snapshot at $t = 4.69$, on the upper side of the galaxy). This large-scale behaviour translates into the characteristics of the SFHs of the spherical models discussed before: large SF peaks separated by quiescent periods.

4.3.2 *Flattened simulations*

The structure of the gas in the flattened dwarf galaxies is quite similar to the spherical ones. Large-scale behaviour with a centralized structure is still very much the case, which again can be connected to the discussion and conclusions about the SFHs of the flattened galaxies. Small-scale structure is not significantly more present than in the spherical models, and the previous discussion of the evolution of the spherical models is equally valid for the initially flattened, non-rotating models.

4.3.3 *Rotating simulations*

The structure of the gas content of the simulated dwarf galaxies is noticeably different when adding rotation. There is now much more small-scale structure in the gas. A 'bubble structure' emerges in the gas, caused by the stellar feedback of individual star particles (snapshot at $t = 0.29$) or small pockets of star particles (very clear at e.g. $t = 6.84$). Apparently, the influence of stellar feedback has become more *local*, and the gas does not exhibit the same *global*, large-scale behaviour seen in the rotationless models.

There is now a very strong difference in the correlation between the local gas density and the separate stellar populations. The newest stars are always found in the densest regions of the gas, which is not illogical considering the SF criteria (Valcke et al. 2008). The slightly older stars are much more likely to be found in the bubbles or holes because individual groups of star particles have had sufficient time to accumulate enough collective feedback. This all speaks in favour of the multi-age model of Weisz et al. (2009) for creating H I holes, and the findings of Stewart et al. (2000) that young stars (Hα) prefer high-density H I regions while older stars (FUV) are more likely found in low-density regions. The idea that UV should be a better tracer for H I holes than Hα therefore seems very plausible. We can also spot cases of triggered secondary SF, the clearest example being at $t = 4.69$ where a large bubble at the lower left-hand side expands outwards and compresses the gas along a rim on the outside of the bubble, spawning new SF in this rim. Observational evidence for similar events can be found where secondary SF is detected in Hα along rims around H I holes (Stewart et al. 2000; Book et al. 2008).

All this again translates into the SFH characteristics we discussed before for rotating dwarf galaxies, where the periodicity, or in other words the large-scale oscillation, of the SFHs from the spherical models is significantly reduced. At times when in the spherical and flattened models SF has almost completely ceased, the rotating model still shows a significant activity. It continuously forms stars throughout the entire simulation.

As a last point, the SF is also noticeably more spatially extended than in the spherical and flattened cases. Moreover, the spatial extent is quite constant during the entire simulation. Stars are always formed throughout practically the entire body of the galaxy, while in the spherical/flattened cases the subsequent SF bursts become increasingly centrally concentrated.

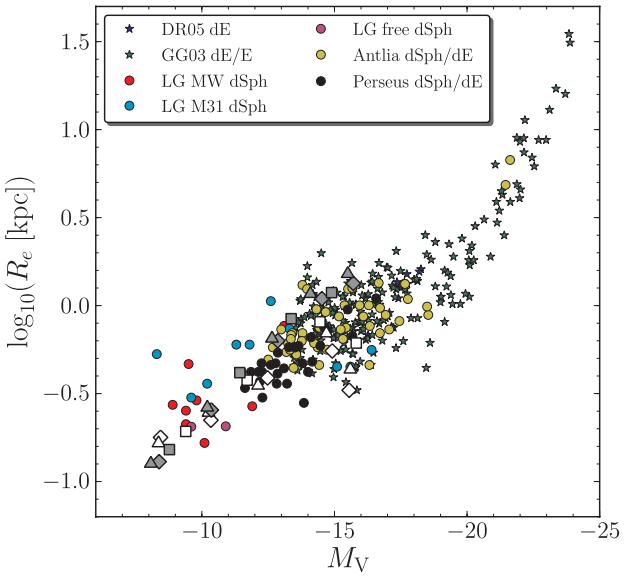

Figure 12. Half-light radius versus V magnitude. White symbols are our non-rotating galaxies; the grey ones are the fastest rotating galaxies (see text). All other points on the plot are observational data found in De Rijcke et al. (2009): LG data come from Peletier & Christodoulou (1993), Irwin & Hatzidimitriou (1995), Saviane, Held & Piotto (1996), Grebel et al. (2003), McConnachie & Irwin (2006), McConnachie, Arimoto & Irwin (2007) and Zucker et al. (2007), Fornax data from Mieske et al. (2007), Antlia data from Smith Castelli et al. (2008), Perseus data from De Rijcke et al. (2009) and other data from Graham et al. (2003) (GG03), De Rijcke et al. (2005) (DR05). The symbol shapes distinguish the initial halo flattenings: simulations with $q = 1$ are shown with lozenges, $q = 0.5$ with triangles and $q = 0.1$ with squares.

4.4 Scaling relations

Aside from the specific characteristics of individual models we discussed above, we also consider the global photometric and kinematical scaling relations traced by the simulated galaxies. Our main aim is to see how well the general characteristics of our simulated dwarf galaxies agree with observational data of dwarf galaxies as a class.

In the following, two series of simulations are plotted. First, all non-rotating galaxy models, both with spherically symmetric and with flattened haloes, represented with white symbols in Figs 12–19. Secondly, all galaxy models initially rotating at $v_{\rm rot} = 5\,{\rm km\,s^{-1}}$, both with spherically symmetric and with flattened haloes, are represented with grey symbols in these figures. The symbol shapes distinguish the initial halo flattenings: simulations with $q = 1$ are shown with lozenges, $q = 0.5$ with triangles and $q = 0.1$ with squares. See Tables 2 and 3.

4.4.1 *Half-light radius* $R_{\rm e}$

The effects of flattening and rotation on the half-light radius are clear in Fig. 12, where $R_{\rm e}$ versus M_V is shown. Overall, at a fixed

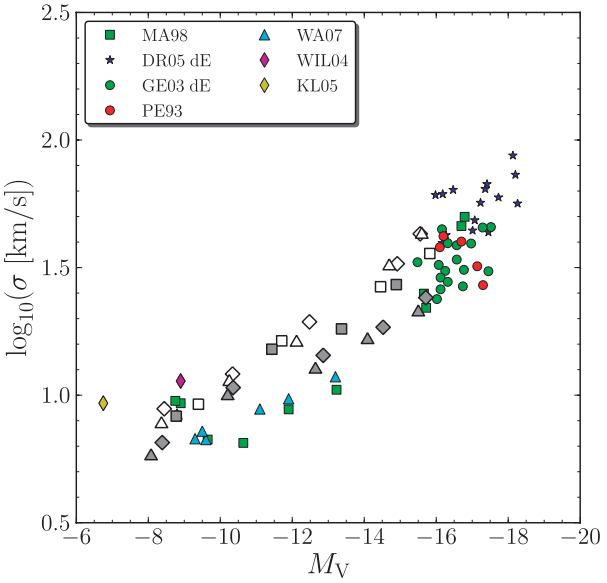

Figure 13. Stellar velocity dispersion versus V magnitude. Observational data: Mateo 1998 (MA98), De Rijcke et al. 2005 (DR05), Geha et al. 2003 (GE03), Peterson & Caldwell 1993 (PE93), seven MW dSphs from Walker et al. 2007 (WA07), Ursa Minor from Wilkinson et al. 2004 (WIL04) and Ursa Major from Kleyna et al. 2005 (KL05).

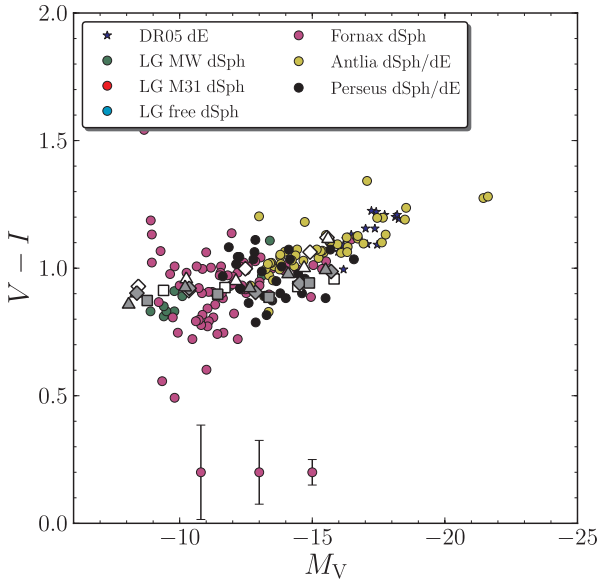

Figure 14. $V-I$ colour versus V magnitude. Symbols as in Fig. 12, and the typical error bars for the Fornax cluster dSph data are shown. Observational data as in Fig. 12.

luminosity, rotation causes R_e to increase. The initial flattening of the halo does not seem to make a significant difference since both model sequences are quite narrow. Only at the high-mass end of the non-rotating series does R_e increase with flattening, the rotating series are unaffected. Overall, there does not seem to be a second parameter effect. Both series together nicely encompass the observational width of the scaling relation. The third series of simulations (with a low initial rotation speed of $v_\mathrm{rot} = 1\ \mathrm{km\ s^{-1}}$) were omitted for clarity of the plot. They simply lie between the two plotted series, providing us with rotation as a possible explanation for the width of the scaling relation.

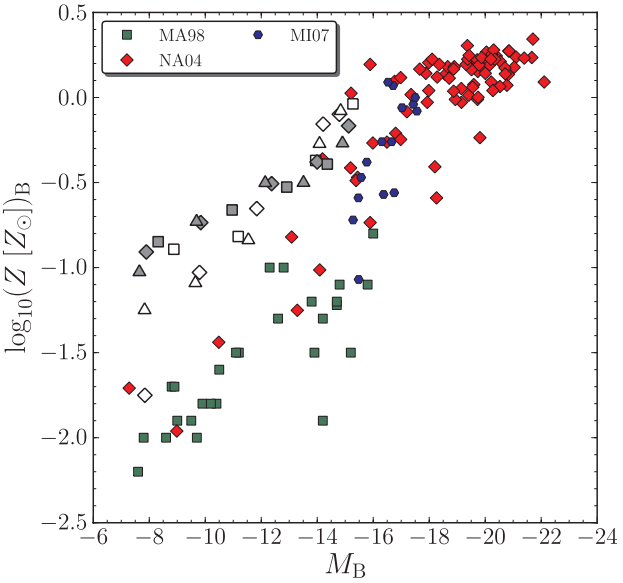

Figure 15. Metallicity in $\log_{10}(Z\,[Z_\odot])_B$ (weighed with B-band luminosity, with $Z_\odot = 0.02$) versus B magnitude. Data: Mateo 1998 (MA98), Nagashima & Yoshii 2004 (NA04) and Michielsen et al. 2007 (MI07).

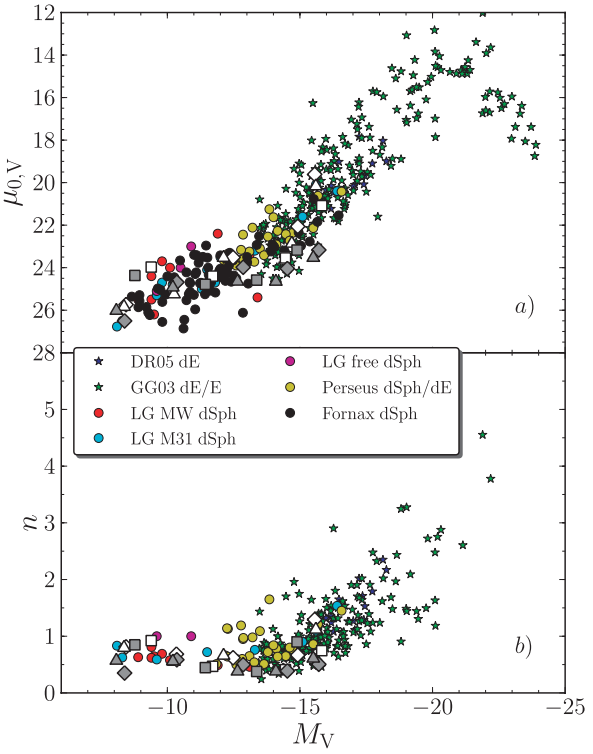

Figure 16. Sérsic parameters versus V magnitude. Upper panel: central surface brightness μ_0 in the V band; lower panel: Sérsic index n. Observational data as in Fig. 12.

4.4.2 *Velocity dispersion σ*

Fig. 13 shows the stellar central velocity dispersion σ versus M_V, projected along the line of sight. We take this to be the x-axis, viewing the models edge-on. As in Valcke et al. (2008), the central velocity dispersion is in general somewhat too high. However, the rotating models, having lower velocity dispersions, compare

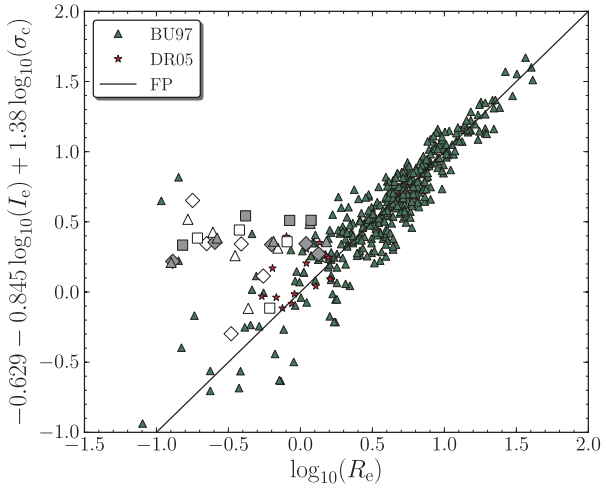

Figure 17. Side view of the Fundamental Plane in physical coordinates. White symbols are our non-rotating galaxies; the grey ones are the fastest rotating galaxies, shapes denote initial flattening as in Fig. 12. All other points on the plot are observational data, taken from Burstein et al. 1997 (BU97) and De Rijcke et al. 2005 (DR05).

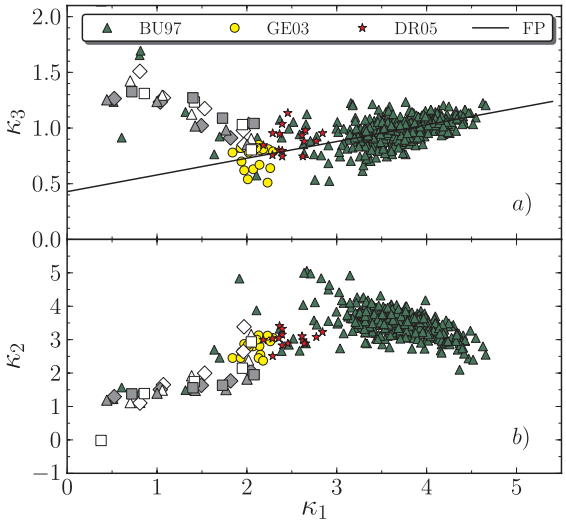

Figure 18. The Fundamental Plane in κ-space. Upper panel: side view of Fundamental Plane (κ_3, κ_1); lower panel: face-on view (κ_2, κ_1). Observational data from Geha et al. 2003 (GE03), other symbols as in Fig. 17.

favourably to spherically symmetric or flattened ones. This decrease of the velocity dispersion in the more massive models is tied to the increase of the half-light radius in the more massive models. In the rotating series the initial flattening also appears to have somewhat of an effect, leading to slightly higher velocity dispersions in the most flattened cases (squares). This is possibly due to the high M/L ratio of these systems, since they have a considerably higher dynamical mass (for a given stellar mass) than their initially less flattened counterparts (see Table 3).

4.4.3 Colour $V - I$

The global $V - I$ colours of the models are shown in Fig. 14. The rotating galaxies lie a little lower than the non-rotating on this plot, meaning these galaxies are slightly bluer. This can be understood from their SFHs (Fig. 9). The strength of the first SF peak

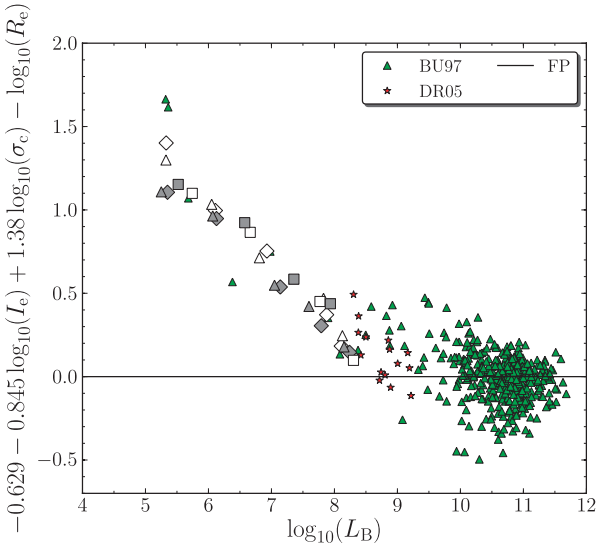

Figure 19. Deviation from the Fundamental Plane. Symbols as in Fig. 17.

is reduced, while at later times SF is enhanced with respect to the non-rotating case, producing more younger, bluer stars. Otherwise, all simulations fall well within the observational range. This is, however, not a very stringent test of the models, given the fact that the $V - I$ colour of an intermediate-age stellar population is relatively insensitive to metallicity (see next paragraph).

4.4.4 Metallicity

The metallicity of all dwarf models is too high, especially in the low-mass regime. This problem was already encountered by Valcke et al. (2008) for the spherically symmetric models. Below $M_B \approx -12$ mag, the rotating models are more metal rich than non-rotating ones whereas above this magnitude they are less metal rich. An explanation for the low-mass models can again be found in the respective SFHs (Fig. 9). In the least massive non-rotating models, the large first peak in the SFH strongly inhibits further SF because the combined force of the feedback is strong enough to severely lower the gas density. Adding rotation reduces this first peak and thus also its truncating power, allowing SF to proceed continuously and enrich the gas further with subsequent stellar generations. When going to higher masses however, the effect and importance of the first peak decreases. From the C07 model on, the trend reverses. This is most likely due to the strong decrease in central concentration of SF and feedback because of rotation (see Figs 11 and 20), together with the simple fact that less stellar mass is produced. SF, metal production and gas enrichment are much more diffuse, providing (on average) less metal-rich gas for subsequent stellar generations.

4.4.5 Surface brightness profiles

The surface brightness profiles are fitted with a Sérsic law,

$$I(R) = I_0 \mathrm{e}^{-(R/R_0)^{1/n}}, \tag{7}$$

from which the parameters μ_0 and n are plotted and compared with observational data in Fig. 16. The Sérsic index n does not differ significantly between rotating and non-rotating models. The central surface brightness μ_0, on the other hand, is consistently lower in the rotating models. This is to be expected: with rotation

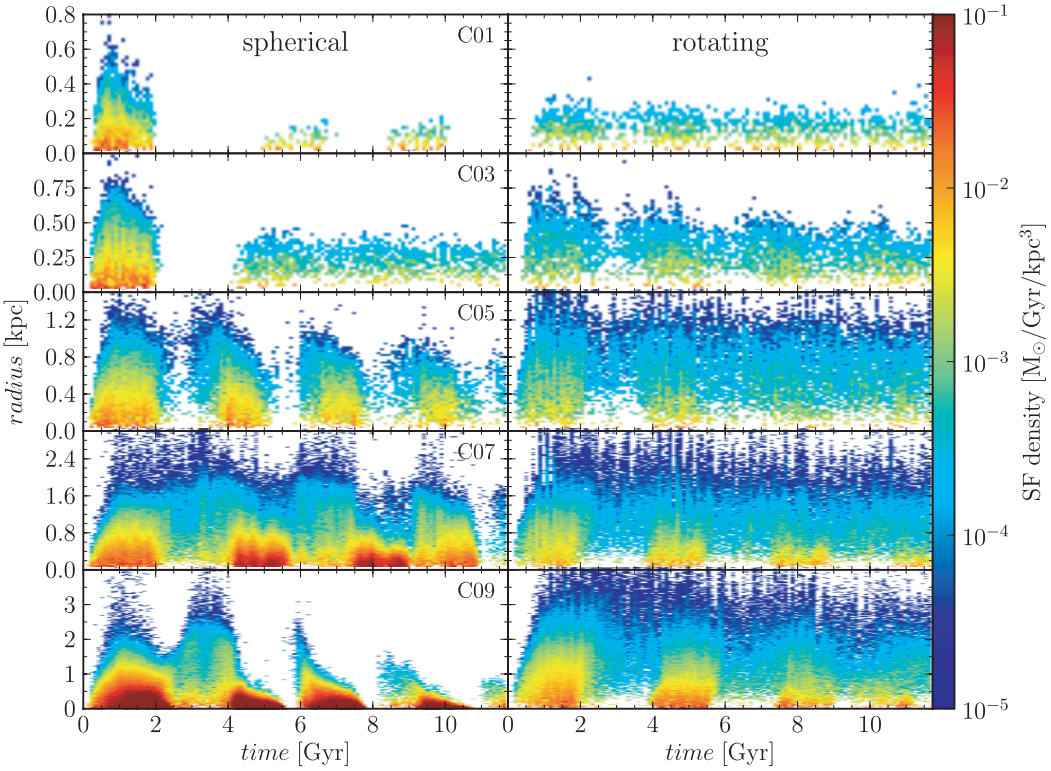

Figure 20. SF density in $M_\odot\,Gyr^{-1}\,kpc^{-3}$ for spherical, non-rotating (left-hand column) and rotating models (right-hand column). The total mass of the models increases from the top down as indicated in the figure. SF density is plotted in colour code versus time on the *x*-axis and radius on the *y*-axis.

the SF becomes less centrally concentrated and more widespread, lowering the central surface brightness.

4.4.6 Fundamental Plane

The Fundamental Plane (Bender, Burstein & Faber 1992; Burstein et al. 1997) is shown in physical coordinates (Fig. 17) and in κ space (Fig. 18). The 'vertical' deviation from the Fundamental Plane is shown in Fig. 19. Except for the most massive non-rotating galaxy models (white lozenges), which are very compact, most dwarf galaxy models lie significantly above the Fundamental Plane. These compact non-rotating dwarfs have small R_e and consequently high mean surface brightness within R_e (denoted by I_e), making them stick out in the side-view of the Fundamental Plane (Fig. 17) and in its κ_1–κ_2 projection (Fig. 18).

Overall, the simulations agree very well with the observational trends and luminosity-dependent deviations from the Fundamental Plane (observational data taken from Burstein et al. 1997). Even the compact non-rotating models fall within the observational spread of the relation.

5 RESULTS/DISCUSSION

5.1 Evaluation of analysis

From the previous paragraph, it is clear that rotation has a more pronounced influence on the observational properties of the simulated dwarf galaxies, quantified by photometric and kinematical scaling relations, than the flattening of the initial conditions. The differences *between* the sequences of rotating and non-rotating models are significantly larger than those between flattened and non-flattened galaxies *within* each sequence. Still, all models fall within the range allowed by the data, apart from the problems we noted with metallicities being to high. Moreover, despite their simplicity, this suite of simulations suggests a possible explanation for the widths of the observed scaling relations. While mass is the dominant parameter that determines the shape and slope of each scaling relation, angular momentum could be an important second parameter that determines the width of the relations. This will however not be the only factor, since external influences such as environment and merger history are likely to also have a significant influence here. Furthermore, we should also note the inherent variance that is present in our models, as discussed in Section 3.3.1 and shown in Fig. 2.

While the effects of flattening and rotation on the observed scaling relations are modest, the addition of rotation has a strong effect on the details of the evolution of dwarf galaxies. This is most clearly seen in the properties of the stellar populations, e.g. in the metallicity profiles (Figs 7 and 8), SFHs (Figs 9 and 10) and overall appearances (Fig. 11). In this respect, rotating models are qualitatively quite distinct from non-rotating ones, independent of initial flattening: rotating models have continuous SFHs with widespread SF while non-rotating models have 'breathing' SFHs with centrally concentrated SF. Observationally, this leads to rotating models having flat metallicity profiles while non-rotating models show pronounced negative metallicity gradients.

5.2 Mechanism

Within the sequence of non-rotating models, flattening of the initial conditions appears to have very little effect on the models' properties, which is of importance especially when considering the metallicity profiles. It therefore seems doubtful that the fountain mechanism is very important for dwarfs. Still, if there are large

feedback driven outbursts of gas, they tend to be aligned preferentially along the minor axis. But the expelled enriched gas does not fall back on to the galaxy. This is most likely because of the shallow potential wells of dwarf galaxies, and because the remaining cold gas is simply 'in the way'. Another important argument against the fountain mechanism is the actual flattening of dwarf galaxies, both in observations and in our simulations, as we discussed in Section 3.3.3. Dwarf galaxies simply are not likely to occur with very flat shapes (Sánchez-Janssen et al. 2010). Their flattenings are not comparable to those of massive spiral galaxies ($q \approx 0.2$), they are on average much thicker ($\langle q \rangle \approx 0.6$). This often makes it difficult to even speak of a 'disc' in the context of dwarf galaxies. Therefore, while the fountain mechanism might be very relevant in the domain of large spiral galaxies, with much deeper potential wells and much flatter shapes, it does not appear an important mechanism in dwarf galaxies.

Rotation, on the other hand, leads to important qualitative and quantitative changes in the SFHs of dwarfs. The consequences of the addition of angular momentum are the following.

(i) Gas will spiral inward, instead of falling straight to the centre. There is a '*centrifugal barrier*' preventing the gas from collapsing to a dense central region.

(ii) Since the gas density is much more smeared out, so is the star formation. The density criterion (see Section 2.1.1) for SF is now reached in a much larger region of the gas, so that SF will occur throughout practically the entire body of the galaxy. This is evident in Figs 11 and 20: SF is consistently more spatially extended in comparison with non-rotating models.

(iii) This naturally produces more spatially homogeneous stellar populations. Therefore the gas is enriched much more homogeneously across the entire galaxy, explaining the flat metallicity profiles in Fig. 7.

(iv) Where there is SF, unavoidingly there will also be stellar feedback. Since the former is smeared out across almost the entire galaxy, so is the latter. The supernova feedback now being less centrally concentrated, this leads to much less pronounced large-scale collective behaviour of the gas. The effects of feedback are now more *local*. This has two distinct but related effects.

(a) The supernovae combine their energy locally on a smaller scale, and produce *low-density holes* in the gas, instead of collectively blowing out the gas and lowering the global gas density after a large centralized SF event. This hole or bubble structure is clearly visible in Fig. 11 and is discussed in Section 4.3.

(b) This can also be linked to our findings concerning the SFHs in Section 4.2 and Fig. 9. Since the gas does not collectively blow out due to feedback, star formation will not shut down completely across the entire galaxy, because only locally the density criterion for star formation is not satisfied (in the feedback holes, Fig. 11). This is also seen in Fig. 20. Collective behaviour – i.e. large-scale oscillations in the SFR – is diminished, leading to more continuous, less variable SFH. The 'breathing' SF, typical of non-rotating models, is largely absent.

The density criterion mentioned in Section 2 and here in point (ii) is an important element of our models. We should note that we employ a threshold of $0.1\,\mathrm{cm}^{-3}$, while Governato et al. (2010) suggest the usage of a threshold of $100\,\mathrm{cm}^{-3}$, reflecting more realistically the conditions of real star-forming gas clumps. We do not expect this to qualitatively change the proposed mechanism however: the higher threshold will take the gas longer to reach it when collapsing, but the extension of the cooling curves below 10^4 K (Maio et al. 2007) will cause the gas to collapse easier and on smaller scales. These effects might not cancel each other out, but the relative influence of added rotation, as discussed above, will remain qualitatively similar. Perhaps on small scales the chemical homogeneity will be less, but on large scales rotating galaxies will still be chemically homogeneous. The inclusion of the high-density threshold and the extra cooling will be the subject of further research.

5.3 Galaxy types

As already mentioned in Section 4.4, our dwarf galaxy models agree quite well with the observed the scaling relations of early-type galaxies. However, since the model galaxies still contain gas and have ongoing SF at the end of the simulation, they should be classified as late-type dwarfs.

5.3.1 dIrrs?

The non-rotating and slowly rotating models, both flattened and non-flattened, are characterized by

(i) centrally concentrated gas distribution, high central density;
(ii) low specific angular momentum;
(iii) strong stellar population gradients;
(iv) bursty or episodic SF,
(v) centrally concentrated SF,
(vi) large-scale feedback driven outflows and a largely featureless ISM.

The fast rotating models, both flattened and non-flattened, are characterized by

(i) spatially extended gas distribution, low central density;
(ii) high specific angular momentum;
(iii) small stellar population gradients, if any;
(iv) continuous SF;
(v) small star-forming regions, scattered across the galaxy;
(vi) turbulent ISM with distinct feedback-driven holes.

dIrrs are known to have a more extensive and less centrally concentrated gas distribution than other gas-rich dwarf galaxy types (e.g. BCDs), and also a relatively high specific angular momentum. Chemical homogeneity is a general trait of dIrrs, both in their gas and their stellar content (Kobulnicky & Skillman 1997; Tolstoy et al. 2009). From the review of dwarf galaxy properties in Tolstoy et al. (2009) and the extensive work of Dolphin et al. (2005), using colour–magnitude diagram (CMD) analysis to reconstruct dwarf galaxy SFHs (Tosi et al. 1991; Aparicio et al. 1996; Tolstoy & Saha 1996; Dolphin 1997, 2002), it is clear that dIrrs generally have a 'continuous' SFH without quiescent periods without SF. The characteristic gas structures of dIrrs have already been discussed in Section 4.3.

From this short overview of the observed properties of late-type dwarfs, it is clear that our fast rotating models resemble dIrrs, at least qualitatively. But our non-rotating and slowly rotating models do not, although they do also still contain gas and show ongoing (periodic) SF. Angular momentum, it seems, invokes different SF modes in dwarf galaxies. It differentiates between centralized/bursty and extended/continuous SF, and all dwarf galaxy properties connected with this which are mentioned above. Although quantitatively not comparable to our models, it is worth mentioning BCDs and their

differences with dIrrs. They too are gas-rich late-type dwarf galaxies, but have a lower specific angular momentum and much more concentrated gas distribution (van Zee et al. 2001; van Zee 2002). BCDs also show substantial colour gradients (van Zee 2002), indicating chemical inhomogeneity, and by definition have bursting SFHs.

5.3.2 Conversion of late-type dwarfs to early types

Since internal processes such as supernova feedback are not capable of removing the gas from a dwarf galaxy, we turn to external or environmental processes, e.g. tidal stripping and ram-pressure stripping (Mayer et al. 2006). Ram-pressure stripping is able to remove a large fraction of the gas and leaves the structure and kinematics of the stars relatively undisturbed, thus preserving any pre-existing stellar population gradients and rotation (Grebel, Gallagher & Harbeck 2003; Marcolini, Brighenti & D'Ercole 2003). Tidal interactions can cause violent reactions in dynamically cold thin-disc dwarf galaxies and can significantly disturb them (Mayer et al. 2001a,b). However, the majority of the dwarf late-type population is quite round, with mean axial ratio $\langle q \rangle \approx 0.6$. In such galaxies, tidal interactions wreak much less havoc (Valcke 2010).

We therefore argue that it is possible to convert late-type dwarfs into early-type ones inside a cluster environment by removing their gas and halting SF without significantly altering their structural and kinematical properties (supported by e.g. Toloba et al. 2011). So the rotation which is present in dIrrs can be preserved in their dE descendants along with the stellar characteristics connected with rotation (metallicity profiles).

6 CONCLUSION

The centrifugal barrier mechanism formulated in Section 5 is able to combine all our findings we discussed in the analysis into one coherent picture, emphasizing the importance of rotation in dwarf galaxy behaviour.

6.1 Metallicity profiles

Our interest in this subject was triggered initially by the finds of Koleva et al. (2009), who found that dwarf early-type galaxies without stellar population gradients were also the fastest rotating ones. We conclude from our simulations that (in isolation) rotation, or the absence thereof, is indeed a key factor in creating stellar population gradients. The 'fountain mechanism' does not seem relevant on the scale of dwarf galaxies, and our simulations clearly indicate that the *geometry* or *flattening* of a dwarf galaxy does not have any significant influence: pressure-supported, non-rotating systems behave very much alike, independent of flattening.

We therefore propose the alternative 'centrifugal barrier mechanism' in Section 5.2, which explains the existence of flat metallicity profiles as a natural consequence of its rotation.

6.2 Angular momentum as second parameter

We suggest angular momentum as being a crucial *second parameter* in determining the appearance and evolution of dwarf galaxies, with the total galaxy mass being the prominent first parameter. While our simulations are admittedly very idealized and cannot purport to paint a cosmologically up-to-date picture of dwarf galaxy formation, they have the enormous benefit of allowing us to unambiguously identify the influence of individual parameters, such as angular momentum.

We have shown that rotation has a significant impact on the stellar populations of dwarf galaxies. And in the same vein we can say the opposite for dwarf galaxy flattening, which shows no significant influence in our simulations, and thus is less likely to be a major player in dwarf galaxy evolution.

6.3 Making dIrrs

We find that without rotation, it does not seem possible to qualitatively produce 'typical' dIrrs with spatially extended SF, continuous SFHs, a turbulent ISM with low-density holes and most importantly with chemical homogeneity throughout its body of gas and stars. Non-rotating models do not display any of these characteristics (having centralized SF, bursty SFHs, featureless ISMs and metallicity gradients). Angular momentum appears to differentiate between bursty and continuous SF modes.

ACKNOWLEDGMENTS

We wish to thank the anonymous referee for the many helpful comments and suggestions which improved this paper. We also thank Volker Springel for making publicly available the GADGET-2 simulation code. JS thanks the Fund for Scientific Research – Flanders, Belgium (FWO) for financial support. All simulations were run on our local computer cluster ITHILDIN.

REFERENCES

Alard C., 2001, A&A, 377, 389
Aparicio A., Gallart C., Chiosi C., Bertelli G., 1996, ApJ, 469, L97
Barazza F. D., Binggeli B., 2002, A&A, 394, L15
Barazza F. D., Binggeli B., Jerjen H., 2002, A&A, 391, 823
Battaglia G. et al., 2006, A&A, 459, 423
Battaglia G., Tolstoy E., Helmi A., Irwin M., Parisi P., Hill V., Jablonka P., 2011, MNRAS, 411, 1013
Bender R., Burstein D., Faber S. M., 1992, ApJ, 399, 462
Bernard E. J., Aparicio A., Gallart C., Padilla Torres C. P., Panniello M., 2007, AJ, 134, 1124
Binggeli B., Popescu C. C., 1995, A&A, 298, 63
Binggeli B., Tammann G. A., Sandage A., 1987, AJ, 94, 251
Book L. G., Chu Y.-H., Gruendl R. A., 2008, ApJS, 175, 165
Burstein D., Bender R., Faber S., Nolthenius R., 1997, AJ, 114, 1365
Buyle P., De Rijcke S., Michielsen D., Baes M., Dejonghe H., 2005, MNRAS, 360, 853
Cioni M.-R. L., 2009, A&A, 506, 1137
Conselice C. J., O'Neil K., Gallagher J. S., III, Wyse Rosemary F. G., 2003, ApJ, 591, 167
Côté S., Carignan C., Freeman K. C., 2000, AJ, 120, 3027
Côté S., Draginda A., Skillman E. D., Miller B. W., 2009, AJ, 138, 1037
Dejonghe H., de Zeeuw T., 1988, ApJ, 333, 90
De Looze I. et al., 2010, A&A, 518, L54
den Brok M. et al., 2011, MNRAS, doi:10.1111/j.1365-2966.2011.18606.x
De Rijcke S., Zeilinger W. W., Dejonghe H., Hau G. K. T., 2003a, MNRAS, 339, 225
De Rijcke S., Dejonghe H., Zeilinger W. W., Hau G. K. T., 2003b, A&A, 400, 119
De Rijcke S., Michielsen D., Dejonghe H., Zeilinger W. W., Hau G. K. T., 2005, A&A, 438, 491
De Rijcke S., Penny S. J., Conselice C. J., Valcke S., Held E. V., 2009, MNRAS, 393, 798
De Young D. S., Gallagher J. S., III, 1990, ApJ, 356, L15
De Young D. S., Heckman T. M., 1994, ApJ, 431, 598
Dolphin A., 1997, New Astron., 2, 397
Dolphin A. E., 2002, MNRAS, 332, 91

Dolphin A. E., Weisz D. R., Skillman E. D., Holtzman J. A., 2005, preprint (astro-ph/0506430)
Dufour R. J., Harlow W. V., 1977, ApJ, 216, 706
Ferguson H. C., Binggeli B., 1994, A&AR, 6, 67
Ferrara A., Tolstoy E., 2000, MNRAS, 313, 291
Geha M., Guhathakurta P., van der Marel R. P., 2003, AJ, 126, 1794
Governato F. et al., 2010, Nat, 463, 203
Graham A. W., Jerjen H., Guzmán R., 2003, AJ, 126, 1787
Grebel E. K., Gallagher J. S., III, Harbeck D., 2003, AJ, 125, 1926
Harbeck D. et al., 2001, AJ, 122, 3092
Hernández-Martínez L., Peña M., Carigi L., García-Rojas J., 2009, A&A, 505, 1027
Hunter D. A., Elmegreen B. G., 2006, ApJS, 162, 49
Irwin M., Hatzidimitriou D., 1995, MNRAS, 277, 1354
Jerjen H., Kalnajs A., Binggeli B., 2000, A&A, 358, 845
Kaufer A., Venn K. A., Tolstoy E., Pinte C., Kudritzki R.-P., 2004, AJ, 127, 2723
Kaufmann T., Wheeler C., Bullock J. S., 2007, MNRAS, 382, 1187
Kim S., Dopita M. A., Staveley-Smith L., Bessell M. S., 1999, AJ, 118, 2797
Kim S., Staveley-Smith L., Dopita M. A., Sault R. J., Freeman K. C., Lee Y., Chu Y., 2005, preprint (astro-ph/0506224)
Kleyna J. T., Wilkinson M. I., Evans N. W., Gilmore G., 2005, ApJ, 630, L141
Kobulnicky H. A., Skillman E. D., 1997, ApJ, 489, 636
Koleva M., de Rijcke S., Prugniel P., Zeilinger W. W., Michielsen D., 2009, MNRAS, 396, 2133
Lianou S., Grebel E. K., Koch A., 2010, A&A, 521, A43
Lisker T., Glatt K., Westera P., Grebel E. K., 2006, AJ, 132, 2432
McConnachie A. W., Irwin M. J., 2006, MNRAS, 365, 1263
McConnachie A. W., Arimoto N., Irwin M., 2007, MNRAS, 379, 379
McCray R., Kafatos M., 1987, ApJ, 317, 190
Mac Low M.-M., Ferrara A., 1999, ApJ, 513, 142
Maio U., Dolag K., Ciardi B., Tornatore L., 2007, MNRAS, 379, 963
Marcolini A., Brighenti F., D'Ercole A., 2003, MNRAS, 345, 1329
Mateo M. L., 1998, ARA&A, 36, 435
Mayer L., Governato F., Colpi M., Moore B., Quinn T., Wadsley J., Stadel J., Lake G., 2001a, ApJ, 547, L123
Mayer L., Governato F., Colpi M., Moore B., Quinn T., Wadsley J., Stadel J., Lake G., 2001b, ApJ, 559, 754
Mayer L., Mastropietro C., Wadsley J., Stadel J., Moore B., 2006, MNRAS, 369, 1021
Michielsen D. et al., 2007, ApJ, 670, L101
Mieske S., Hilker M., Infante L., Mendes de Oliveira C., 2007, A&A, 463, 503
Nagashima M., Yoshii Y., 2004, ApJ, 610, 23
Pagel B. E. J., Edmunds M. G., Fosbury R. A. E., Webster B. L., 1978, MNRAS, 184, 569
Peletier R. F., Christodoulou D. M., 1993, AJ, 105, 1378
Pelupessy F. I., van der Werf P. P., Icke V., 2004, A&A, 422, 55
Penny S. J., Conselice C. J., De Rijcke S., Held E. V., 2009, MNRAS, 393, 1054
Peterson R. C., Caldwell N., 1993, AJ, 105, 1411
Revaz Y. et al., 2009, A&A, 501, 189
Rhode K. L., Salzer J. J., Westpfahl D. J., Radice L. A., 1999, AJ, 118, 323
Roychowdhury S., Chengalur J. N., Begum A., Karachentsev I. D., 2010, MNRAS, 404, L60
Sánchez-Janssen R., Méndez-Abreu J., Aguerri J. A. L., 2010, MNRAS, 406, L65
Saviane I., Held E. V., Piotto G., 1996, A&A, 315, 40
Sawala T., Scannapieco C., Maio U., White S., 2010, MNRAS, 402, 1599
Sawala T., Guo Q., Scannapieco C., Jenkins A., White S., 2011, MNRAS, 413, 659
Schmidt M., 1959, ApJ, 129, 243
Skillman E. D., 2005, New Astron. Rev., 49, 453
Smith Castelli A. V., Bassino L. P., Richtler T., Cellone S. A., Aruta C., Infante L., 2008, MNRAS, 386, 2311
Springel V., 2005, MNRAS, 364, 1105
Staveley-Smith L., Davies R. D., Kinman T. D., 1992, MNRAS, 258, 334
Stewart S. G. et al., 2000, ApJ, 529, 201
Stinson G., Seth A., Katz N., Wadsley J., Governato F., Quinn T., 2006, MNRAS, 373, 1074
Stinson G. S., Dalcanton J. J., Quinn T., Kaufmann T., Wadsley J., 2007, ApJ, 667, 170
Sung E.-C., Han C., Ryden B. S., Patterson R. J., Chun M.-S., Kim H. I., Lee W.-B., Kim D.-J., 1998, ApJ, 505, 199
Sutherland R. S., Dopita M. A., 1993, ApJS, 88, 253
Toloba E., Boselli A., Cenarro A. J., Peletier R. F., Gorgas J., Gil de Paz A., Muñoz-Mateos J. C., 2011, A&A, 526, A114
Tolstoy E., Saha A., 1996, ApJ, 462, 672
Tolstoy E. et al., 2004, ApJ, 617, L119
Tolstoy E., Hill V., Tosi M., 2009, ARA&A, 47, 371
Tosi M., 2007, in Vallenari A., Tantalo R., Portinari L., Moretti A., eds, ASP Conf. Ser. Vol. 374, From Stars to Galaxies: Building the Pieces to Build up the Universe. Astron. Soc. Pac., San Francisco, p. 221
Tosi M., Greggio L., Marconi G., Focardi P., 1991, AJ, 102, 951
Travaglio C., Hillebrandt W., Reinecke M., Thielemann F.-K., 2004, A&A, 425, 1029
Tsujimoto T., Nomoto K., Yoshii Y., Hashimoto M., Yanagida S., Thielemann F.-K., 1995, MNRAS, 277, 945
Valcke S., 2010, PhD thesis, Ghent University
Valcke S., De Rijcke S., Dejonghe H., 2008, MNRAS, 389, 1111
Valcke S., De Rijcke S., Rödiger E., Dejonghe H., 2010, MNRAS, 408, 71
van Zee L., 2002, in Grebel E. K., Brandner W., eds, ASP Conf. Ser. Vol. 285 Modes of Star Formation and the Origin of Field Populations. Astron. Soc. Pac., San Francisco, p. 333
van Zee L., Salzer J. J., Skillman E. D., 2001, AJ, 122, 121
van Zee L., Skillman E. D., Haynes M. P., 2004, AJ, 128, 121
Vazdekis A., Casuso E., Peletier R. F., Beckman J. E., 1996, ApJS, 106, 307
Walker M. G., Mateo M., Olszewski E. W., Gnedin O. Y., Wang X., Sen B., Woodroofe M., 2007, ApJ, 667, L53
Walter F., Brinks E., de Blok W. J. G., Bigiel F., Kennicutt R. C., Thornley M. D., Leroy A., 2008, AJ, 136, 2563
Weaver R., McCray R., Castor J., Shapiro P., Moore R., 1977, ApJ, 218, 377
Weisz D. R., Skillman E. D., Cannon J. M., Dolphin A. E., Kennicutt R. C., Lee J., Walter F., 2009, ApJ, 704, 1538
Wilkinson M. I., Kleyna J. T., Evans N. W., Gilmore G. F., Irwin M. J., Grebel E. K., 2004, ApJ, 611, L21
Zucker D. B. et al., 2007, ApJ, 659, L21

SUPPORTING INFORMATION

Additional Supporting Information may be found in the online version of this article.

Animation. Animation of the simulations presented in Fig. 11.

Please note: Wiley-Blackwell are not responsible for the content or functionality of any supporting materials supplied by the authors. Any queries (other than missing material) should be directed to the corresponding author for the article.

This paper has been typeset from a TEX/LATEX file prepared by the author.